Deep–Sea Research II 227 (2026) 105620

Contents lists available at ScienceDirect

Deep-Sea Research Part II

journal homepage: www.elsevier.com/locate/dsr2

Discovery of a bathyal methane seep field at the north-western Vestnesa Ridge, Fram Strait

Katrin Linse [a,*], Lilian Boehringer [b], Saskia Brix [c,d], Jennifer Dannheim [b], Jonas Hagemann [b], Fereshteh Hemmateenejad [e], Áki Jarl Láruson [f], Giuliana Panieri [g,h], Lydia Anastasia Schmidt [i], Maximilian Schrade [b,j], Carolin Uhlir [b,c,k], Autun Purser [b]

[a] British Antarctic Survey, High Cross, Madingley Road, Cambridge, CB3 0ET, United Kingdom
[b] Alfred Wegener Institute, Helmholtz Centre for Polar and Marine Research, 27570, Bremerhaven, Germany
[c] German Centre for Marine Biodiversity Research (DZMB), c/o Biozentrum Grindel, Martin-Luther-King-Platz 3, D-20146, Hamburg, Germany
[d] University of Hamburg, Faculty of Mathematics, Informatics and Natural Sciences, Department Biology, Institute of Marine Ecosystem and Fishery Science, Marine Ecosystem Dynamics and Management, Germany
[e] Department of Earth and Environmental Sciences, University of Milano-Bicocca, Milano, Italy
[f] Marine & Freshwater Institute, Fornubðir, 220, Hafnarfjöður, Iceland
[g] CNR, Instituto di Scienze Polari, Via Torino 155, 30172, Venezia, Italy
[h] Department of Geosciences, UiT, The Arctic University of Norway, Tromsø, Norway
[i] Institute of Biological Science, University of Rostock, Albert-Einsteinstraße 3, 18059, Rostock, Germany
[j] University of Oulu, P.O.Box 8000, Pentti Kaiteran katu 1, FI-90014, Finland
[k] University of Hamburg (UHH), Institute of Marine Ecosystem and Fishery Science, Hamburg, Germany

ARTICLE INFO

Keywords:
OFOBS
Bacterial mat
Siboglinidae
Methane seep
Ophiuroidea

ABSTRACT

The Vestnesa Ridge at 79°N in the Arctic Fram Strait is known for sub-surface methane hydrate reservoirs and numerous gas emitting pockmarks, with associated microbial and faunal communities on its eastern flank. The expedition MSM95 in 2020 found the first evidence of active methane seepage on the north-western flank of the Vestnesa Ridge in water depths of 1200 to 1375 m. Subsequent investigations during the PS136, MSM108 and PS143/1 expeditions with towed camera, Remotely Operated Vehicle and trawl sampling confirmed the MSM95 early indications. Here we report the first faunal assemblage description of the discovered active methane seep field, named Hœnir seep field. In-situ image analyses of the methane seep field and its active and inactive areas showed a regional community comprising 47 megafaunal taxa. The presence of obligate seep-associated faunal taxa, such as the tube-building siboglinid polychaetes and oligochaetes were interpreted as indicative of active methane seepage in the area. The most frequent taxon observed, ophiuroids in the genus *Ophiocten* Lütken, 1855, occurred in high densities with up to 80 ind. per m^2 in inactive areas but was absent from the seafloor closer than a few meters from bacterial mat or tubeworm forests. The fauna seen in the Hœnir seep field shares most faunal elements with seep fields previously studied on the eastern flank of the Vestnesa Ridge and on the nearby Svyatagor Ridge. For taxonomic identifications of fauna associated with the methane seepage, 95 specimens of 43 selected taxa, mostly ophiuroids, polychaetes and amphipods, were COI barcoded.

1. Introduction

In the Arctic, active seafloor methane seepage has been discovered on the continental shelves and slopes, and around Arctic islands from water depths of less than 100 m to abyssal depths (Åström et al., 2020). Shallow water, <100 m depth, cold seeps were discovered in the Barents, Norwegian and White Seas, and off western Svalbard (Yusupov et al., 2010; Shakhova et al., 2015; Panieri et al., 2024). The macrobenthic communities in these shallow seeps comprise no or minor chemosymbiotic species and community shifts, while contrasts in faunal abundance and biomass with non-methane seepage substrates were observed (Sahling et al., 2003; Baranov et al., 2020; Vedenin et al.,

This article is part of a special issue entitled: LTER HAUSGARTEN published in Deep-Sea Research Part II.

* Corresponding author.
E-mail address: kl@bas.ac.uk (K. Linse).

https://doi.org/10.1016/j.dsr2.2026.105620
Received 27 February 2025; Received in revised form 16 February 2026; Accepted 28 February 2026
Available online 5 March 2026

2020). Deeper methane seeps and associated ecosystems, from about 200 m to 1900 m depth, including mud volcanoes, have been discovered along the continental slopes in the Beaufort, Bering and Norwegian seas, on the Lofoten-Vesterålen margin and around Svalbard (Gebruk et al., 2003; Paull et al., 2015; Mau et al., 2017; Panieri et al., 2017; Sen et al., 2019; Åström et al., 2020; Thorsnes et al., 2023; Argentino et al., 2024; Eilertsen et al., 2025; Rybakova et al., 2025). Eilertsen et al. (2025) confirmed that the community of the 1900 m deep Svyatogor Ridge seep system hosted specialised fauna with were linked with Arctic hydrothermal vents. Several of the methane seep sites around Svalbard have been studied in multiple years, or autonomously monitored to give indications of variability and stability of the seepage (Sahling et al., 2014; Myhre et al., 2016; Dølven et al., 2022). Evidence of abyssal seepage in approximately 3500 m depth associated with the Spitsbergen Transform Fault was initially found acoustically by gas flare mapping (Thorsnes et al., 2023; Chand et al., 2024), with subsequent visual confirmation by remotely operated vehicle (ROV) in-situ imagery and faunal assemblage characterisation (Panieri et al., 2025).

To the west of Svalbard at 79°N in the Fram Strait, the Vestnesa Ridge is an ultraslow spreading sediment-drift ridge reaching its summit at about 1200 m depth, which has been the of subject of comprehensive geological studies on gas hydrate distribution, hydro fluid migration and identified as the shallow water edge of the gas hydrate stability zone (Panieri et al., 2017; Riedel et al., 2020).

The Vestnesa Ridge hosts a deep reservoir of thermogenic methane as well as microbially derived methane (Bünz et al., 2012). Large-sized pockmarks of approximately 700 m diameter, with a 10 m depression depth, occur along the Vestnesa Ridge summit (Panieri et al., 2017). Several active pockmarks with up to 1 km high gas bubble streams have been described (Panieri et al., 2017; Melaniuk et al., 2022). Confirmed active seepage is only known from the eastern side of the sedimentary ridge (Ramachandran et al., 2022). Two of these active pockmarks, Lunde and Lomvi, have been studied for the present-day and paleo-signature of foraminiferan diversity and geochemical parameters (Consolaro et al., 2018; Melaniuk et al., 2022) as well as for assessment of recent benthic assemblages (Åström et al., 2018, 2019). A further, deeper pockmark on the ridge in 1300 m depth was studied by Eilertsen et al. (2025). The substrates in these active seepage areas are characterised by carbonate crust and blocks, dense areas of bacterial mats and siboglinid tubeworms, forming tubeworm forests, thin-layered bacterial mats, and patchy tubeworms in soft sediments (Panieri et al., 2017; Eilertsen et al., 2025). Methane derived authigenic carbonates were observed to be colonised by megafauna such as anemones, stalked hydroids, and bryozoans while seeping soft-bottom areas were colonised by tube worms (Åström et al., 2018). Mobile taxa, including amphipods, gastropods, pycnogonids, starfish and fish, were observed inside and outside of active pockmarks, but individual taxa showed preferences to either active or inactive areas (Åström et al., 2018; Eilertsen et al., 2025). Eilertsen et al. (2025) identified twelve chemosynthetic-based ecosystem specialised species at the Vestnesa Ridge, of which four were shared with Svyatogor Ridge seeps and six with the Loki's Castle vent field. Observed species richness and diversity, infaunal biomass and abundances were 1.5 to 5 times higher in active seepage soft sediment areas then in inactive areas, indicating an enhancement of biodiversity through the chemoautotrophic production (Åström et al., 2018).

The Vestnesa Ridge, flanking the eastern side of the Molloy Deep is part of the German Long-Term Ecological Research (LTER) observatory HAUSGARTEN in the Fram Strait (Soltwedel et al., 2005, Soltwedel, 2023; Soltwedel et al., 2016, 2018; Dannheim and Contribution of the participants, 2025). Central to the HAUSGARTEN is the study of biodiversity, assemblage structures and turnovers of seafloor communities across the region, as well as their abiotic and biotic parameters in the transition zone between the northern North Atlantic and the central Arctic Ocean (e.g. Vedenin et al., 2019; Käß et al., 2021; Gorska et al., 2022; Schnier et al., 2023; Meyer-Kaiser et al., 2025; this DSR special issue). Hydroacoustic seafloor topography and in-situ seafloor image survey data, collected during RV Maria S Merian's expedition MSM95 in 2020 indicated the presence of pockmarks and methane seepage on the north-western flank of the Vestnesa Ridge. Further HAUSGARTEN expeditions on RV Polarstern, PS136 and PS143, visited the area to investigate the extent and faunal assemblages of the predicted methane seep field. Following the use of Nordic mythology names for Arctic seep and vent fields, this predicted methane seep field was named Hœnir after the god, who following the Prose Edda gave reason to man.

The aim of this study is 1) to describe the extent of the methane seepage field on the north-western flank of the Vestnesa Ridge within the HAUSGARTEN area of study 2) to characterise the habitats present by their seafloor substrates and faunal assemblages, and 3) to identify characteristic faunal elements of the methane seepage habitats by DNA barcoding.

2. Material and methods

2.1. Study region

The north-western end of the Vestnesa Ridge (Fig. 1) was part of a wider multibeam swath bathymetry carried out during MSM95 of RV Maria S Merian in 2020 (Purser et al., 2021). The data from this area, within the HG-IV survey box (HAUSGARTEN station four), initiated further investigations to study the topography, habitats, and benthic fauna. During the expeditions MSM108 of RV Maria S. Merian in 2022 and PS136 (in 2023) and PS143/1 (in 2024) of RV Polarstern, the north-western flank of the Vestnesa Ridge was investigated by multibeam hydroacoustics, sidescan sonar, and in-situ imagery by using Autonomous Underwater Vehicle (AUV), Ocean Floor Observation and Bathymetry System (OFOBS) and by collecting physical specimens with Remotely Operated Vehicle (ROV) and epibenthic sledge (EBS) (Fig. 1c–Table 1).

2.2. Bathymetric seafloor surveys

During the expeditions MSM95 and MSM108 onboard RV Maria S Merian, the north-west of the Vestnesa Ridge was mapped with the vessel's hull-mounted Kongsberg EM122 operating at 10.5 to 13 khz echosounder with a set angle of 65° in equidistant mode at a speed of 7 knots (data incorporated into the new regional map presented in Dreutter et al., CURRENT DSRII ISSUE).

Side scan sonar for mapping of target areas identified by the hull-mounted swath bathymetry was carried out by the Alfred Wegener Institute's (AWI) AUV PAUL 3000 and OFOBS during MSM108 and PS136. The AUV PAUL's ARC-scout side scan sonar (Marine Sonic, Atlas America) was operating at the frequencies 600 and 1200 kHz in an altitude of approximately 5 to 6 m. The OFOBS, equipped with a BlueView M900 forward-looking sonar and an Edgetech 2205 bathymetric side scan sonar, was towed at an altitude of approximately 1.5 m and a speed of 0.5 knots (Purser et al., 2019, 2020). The side scan high and low frequency data were processed using CARIS HIPS and SIPS 11.3 software in a UPS South WGS84 N, E (EPSG: 32761) projection.

2.3. In-situ seafloor imaging

In-situ seafloor imagery collected at different altitudes and resolutions by OFOBS in 2022 (MSM108), 2023 (PS136) and 2024 (PS143/1) were investigated for this study. OFOBS was equipped with a 26 megapixel stills camera (iSiTEC, CANON EOS 5D Mark III), high resolution video camera ((iSiTEC, Sony FCB-H11) and four downward facing SeaLight sphere 3150 LED lights positioned in the corners of the main OFOBS frame, with two additional strobe lights (iSiTEC UW-Blitz 250, TTL driven) (Purser et al., 2019). By default, the photo camera records an image about every 20 s, to allow the strobe illumination to charge between images, and observer triggered “hotkey” images were taken in addition to the timed images to record unique features (Isler et al.,

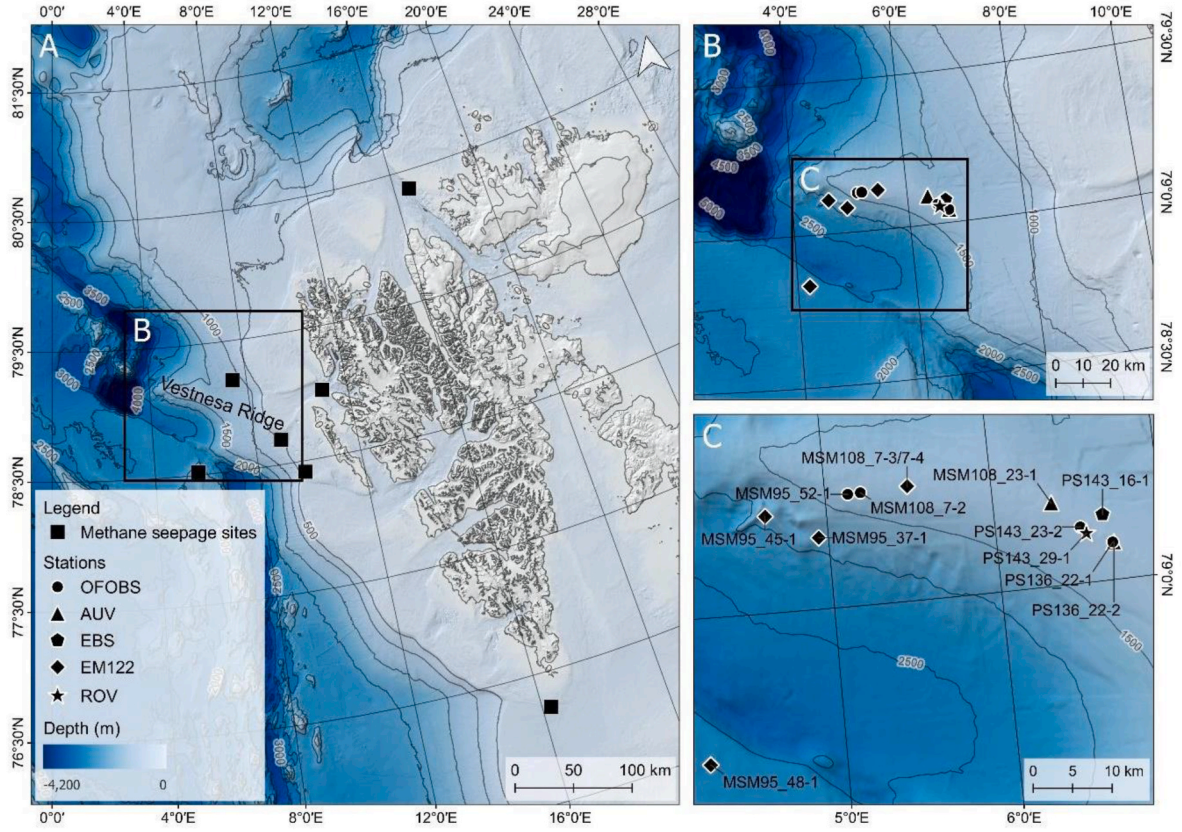

Fig. 1. Map of study area. A) Locations of methane seepage sites (■) around Svalbard. B) regional map of the Vestnesa Ridge. C) Local map of the north-western Vestnesa Ridge showing sampling locations and survey lines. Map source: IBCAO v. 4.0 (Jakobsson et al., 2020). Map was created using QGIS v. 3.26.2-Buenos Aires (QGIS.org, 2019).

Table 1
Station data for the NW Vestnesa Ridge methane seepage area.

Expedition	Station	Date	Gear	Latitude	Longitude	Water depth	Pangaea datasets
				Start	Start	Start	
				°N	°E	(mbsl)	
MSM95	37-1	9/25/2020	EM122	79° 04.854	004° 56,502'	1856	Dreutter et al., 2020, 2022
	45-1	9/28/2020	EM122	79° 06.601'	004° 37.827'	1978	Dreutter et al., 2020, 2022
	48-1	9/30/2020	EM122	78° 50.017'	004° 11.,784'	2367	Dreutter et al., 2020, 2022
	52-1	9/30/2020	OFOBS	79° 07.641'	005° 08,260'	1375	Purser et al., 2021a,b
MSM108	7-2	6/13/2022	OFOBS	79° 07.669'	005° 12.865'	1357	Purser and Boehringer, 2023
	7-3	6/13/2022	EM122	79° 07.790'	005° 29.935'	1301	Soltwedel et al., 2024
	7-4	6/13/2022	EM122	79° 07.820'	005° 29.942'	1304	Soltwedel et al., 2024
	23-1	6/23/2022	AUV	79° 02.551'	006° 41.842'	1221	
PS136	22-1	6/7/2023	OFOBS	79° 02.547'	006° 41.403'	1229	Isler et al., 2024b
	22-2	6/7/2023	AUV	79° 02.551'	006° 41.842'	1229	
PS143/1	16-1	6/23/2024	EBS	79° 04.500'	006° 38.904'	1282	
	23-2	6/27/2024	OFOBS	79° 03.815'	006° 30.506'	1206	Boehringer et al., 2025
	29-1	7/30/2024	ROV	79° 03.341'	006° 32.432'	1736	

2024a). From an altitude of 2 m, both camera images covered an area of approximately 6.5 m^2 of even seafloor. Three red lasers were positioned triangular with 50 cm distance between each other (Purser and Boehringer, 2023).

2.4. OFOBS image analyses

OFOBS images of the expeditions MSM108, PS136 and PS143 (both expedition legs) are submitted to publicly available databases (Table S1). The timed OFOBS images of the expeditions MSM108, PS136 and PS143/1 were analysed regarding the present seafloor cover and megabenthic epifauna while the hotkey images were assessed for seafloor cover and identification of present fauna absent in the timed images. Low quality images (too dark, too high above or too close to seafloor, extensive sediment clouds and too many particles obscuring seafloor) were omitted from the analysis. To account for camera edge lens distortion effects, the images were split into 100 equal rectangles and the outer rectangle layer was excluded, leaving 74 rectangles for analysis, which represent about 2.8 m^2 of analysed seafloor. The images were analysed to access percentage cover of abiotic and biotic substrate types following the sedimentary size classification of Tucker (1991), and specific to the Arctic Ocean following the substrate catalogue by Hemmateenejad et al. (2025a): mud, sand, gravel, pebbles, cobbles, boulders, or bedrock with the addition of bacterial mats, coloured sediments

and carbonates to note methane seepage origins. Epibenthic megafaunal taxa were counted. As image-derived taxonomic identification to lower taxonomic levels is unreliable, we followed the recommendations by Horton et al. (2021), basing the identifications on established phylum and class levels, in selected compelling taxa to family or genus level. For comparability with other Arctic methane seepage associated fauna, we used the taxon code established by Hemmateenejad et al. (2025b) for benthic fauna and fish in the Arctic Ocean and Barent Sea. Taxa, not present in Hemmateenejad et al. (2025b), were given the next numerical taxon codes for the relevant taxon, following the latter catalogue and were marked with "*" in the table listing the observed taxa and imaged in Supplement Material 1.

2.5. Benthic sampling and sample treatment

Macro- and megabenthic specimen samples were collected during PS143/1 by EBS (station 16-1) and ROV Kiel 6000 (station 29-1) (Table 1). The epibenthic sledge (Brenke, 2005) was deployed and towed along the seafloor for 50 min with a varying speed of 0.4 to 1 knots, depending on the vessel's drifting speed. The estimated trawling distance was calculated as described in Soltwedel et al. (2024), covering approximately 2166 m of seafloor. Selected faunal specimens were removed during live sorting for photographing and subsequent fixing in either undenatured 96 % ethanol, RNA-later or frozen at −80 °C. The remaining bulk samples were fixed in pre-cooled 96 % ethanol for later biodiversity analyses. During the ROV Kiel 6000 dive 29-1 in 2024 (PS143/1), faunal samples were collected by the manipulators either by direct grabbing, using a net with 250 µm mesh size, a push core or the slurp sampler. Collected specimens were photographed and fixed in undenatured 96 % ethanol or RNA-later.

Specimens of representative macro-and megafauna were photographed with a digital Canon EOS 5D Mark IV SLR SLR camera, using a mounted macro-objective MP-E65mm f/2.8 1-5x for the macrofauna and an EF50mm f/2.5 Compact objective for the megafauna. Specimens photographed in the present study were deposited in the working collection of the German Centre for Marine Biodiversity Research (DZMB), Senckenberg am Meer, Hamburg.

2.6. DNA barcoding and sequence editing

Selected specimens of the representative macro- and megafauna were designated for molecular barcoding and their DNA extracted onboard RV Polarstern during PS143/1.

DNA extractions were performed within 24 h after specimen fixation onboard RV Polarstern. Tissue samples from selected specimens were taken, avoiding damage to structures critical for potential morphological species identification. DNA was extracted using the NucleoSpin™ Tissue Kit (Macherey-Nagel), following the manufacturer's protocol. DNA aliquots are stored at −80 °C at the German Centre for Marine Biodiversity Research (DZMB), Senckenberg am Meer, Hamburg.

Polymerase chain reaction (PCR) for barcoding marker cytochrome *c* oxidase subunit I (COI) with primer set LCO1490 and HCO2198 (Folmer et al., 1994) was carried out in the LIB – Center for Molecular Biodiversity Research's Molecular Laboratory in Hamburg out using PCR-Beads, illustraTM PuReTaq Ready-To-GoTM (Avantor®; VWR Int. GmbH, Darmstadt, Germany). The total PCR reaction volume was 25 µl per sample, 10 µmol primer concentrations and 2 µl of template DNA were used. Thermal cycling conditions were as follows: initial denaturation: 95 °C, 5 min; denaturation: 38 cycles, 95 °C, 45 s; annealing: 45 °C, 50 s; elongation: 72 °C, 1 min; final elongation: 72 °C, 5 min; cooling at 10 °C. Quality and quantity of amplified product was assessed by gel electrophoresis using 1.5% agarose gels. Successful PCR products were purified using ExoSAP-IT PCR Product Cleanup Reagent (Thermo Fischer ScientificTM) and run on a thermal cycler (incubation: 37 °C, 15 min; enzyme inactivation: 80 °C, 15 min). Double stranded sequencing was carried out by the sequencing facilities Macrogen Europe Inc. (Amsterdam, Zuidoost, The Netherlands) and Eurofins Genomics Germany GmbH (Ebersberg, Germany) using ABI 3730xl sequencers.

Geneious Prime® (Version, 2022.1.1; Biomatters, Auckland, New Zealand; Kearse et al., 2012) was used to edit and assemble forward and reverse chromatograms as well as to check for potential contamination using the implemented NCBI BLAST search tool (Basic Local Alignment Search Tool; Altschul et al., 1990).

Assembled COI sequences were compared to sequences publicly available with NCBI BLAST (Altschul et al., 1990) and with the BIN (Barcode Index Number) System implemented in the Barcode Of Life Datasystem (Ratnasingham and Hebert, 2013; v3.boldsystems.org) for percentage match and to verify taxon identification.

2.7. Substrate category and faunal abundance analysis

The percentage analysis of substrate category and faunal individual counts were displayed in a joint plot created in Microsoft Excel.

3. Results

In 2020, during OFOBS station 52-1 of MSM95 on the north-western Vestnesa Ridge, bacterial mats indicating evidence for seafloor methane seepage were noticed on images (Table 1). AUV mounted sidescan surveys in 2022 (MSM108) and 2023 (PS136) detected the presence of round depressions in the seafloor which were interpreted as active or inactive pockmarks (Fig. 2). In Fig. 2A–C a number of these pockmarks can be seen, which vary in size from 5 to 25 m diameter. The rugosity of these features varied from rather rough to smooth, and the height could reach several meters above the surrounding seafloor.

During MSM108 in 2022, OFOBS station 7-2 covered an image transect line spanning from the HAUSGARTEN observatory image transect at HG-I (HAUSGARTEN station one) to the area of the MSM95_52-1 station, where features indicative of potential methane seepage were first identified. Out of these, 1741 timed images and 72 "hot key" images were taken, of which 414 timed images were in the indicated methane seepage area. Of these 148 images were analysed for percentage of substrate type and visible megafauna counted, with the remaining images either too dark, or taken too close or too far from the seafloor for comparative image analyses.

The OFOBS station 22-1 of PS136 collected a total of 579 timed and 113 hot key images, of which 479 were used for comparative images analyses. The other one hundred images were again either too dark or taken too close or too far from the seafloor for comparative image analyses. OFOBS station 23-2 of PS143/1 collected a total of 841 timed and 122 hot key images, of which 263 were used for comparative images analyses, while 578 images were not of appropriate quality for comparative analysis.

The abiotic and biotic seafloor categories observed on the OFOBS images were mud, gravel, pebbles, cobbles, boulders, coloured sediments, bacterial mats, coloured sediments, and tubeworm forests, which appeared in two types either with non-overgrown tubes of polychaetes or with epifaunal overgrown tubes of polychaetes (Fig. 3).

Most of the analysable images showed 100% of mud (e.g. soft sediment) as seafloor category (MSM95 – 87%; PS136 - 77%; PS143/1 - 76%), while minority of images showed dense patches of worm tubes (MSM95 – 3%; PS136 – 3%; PS143/1 - 6%), black sediment or white bacterial mat patches ((MSM95 – 0%; PS136 - 1%; PS143/1 - 1%).

The biological images analyses of the three OFOBS stations on the north-western Vestnesa Ridge resulted in the identification of 47 taxa, with 19 taxa present in three OFOBS transects of MSM108/PS136/PS143/1 (Table 2). The ophiuroid (OPH_004) was the most abundant and frequent taxon in the analysed images, with over 12,000/47,000/15,000 individuals counted and present in 78%/85%/71% of the images respectively. Ophiuroid abundances reached up to 225 individuals per images, resembling about 80 individuals per m^2. The next abundant and frequent taxa were by sabellid-like polychaetes (ANN_003) (179/657/

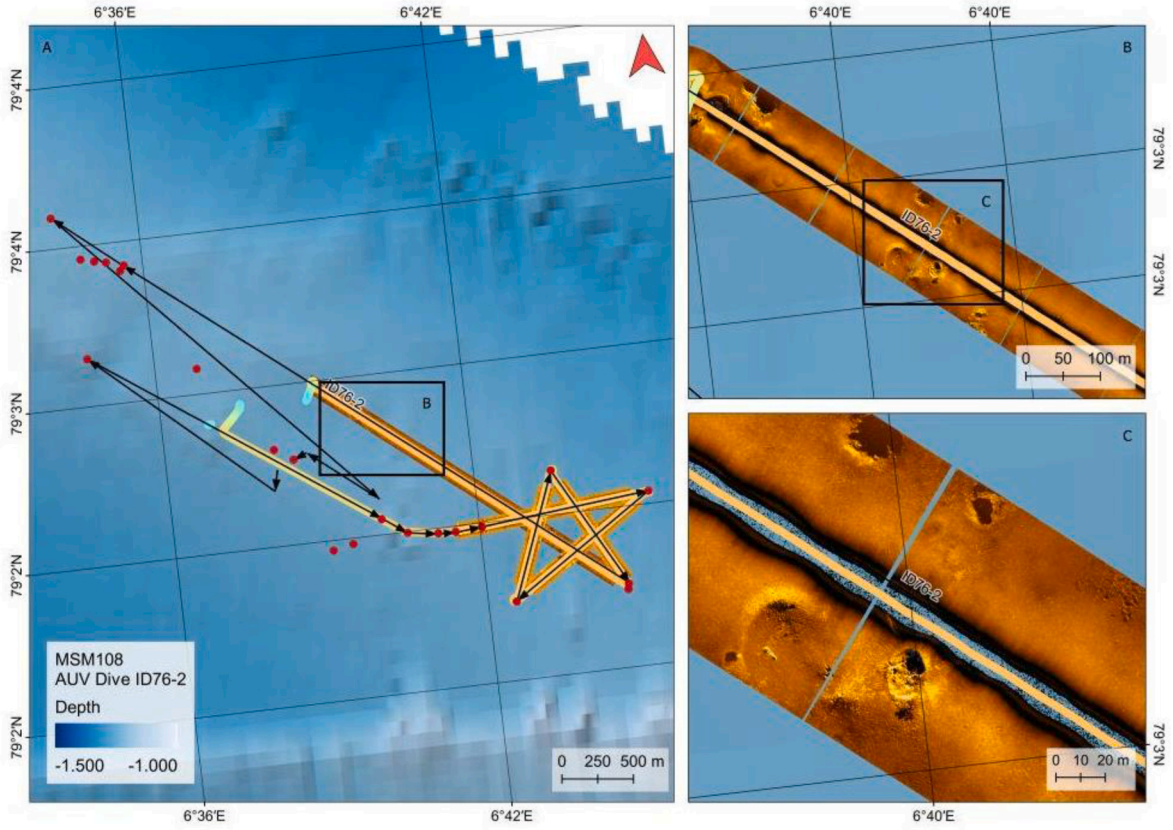

Fig. 2. Horizontal extent of the *Hœnir* methane seep field. A) MSM108 AUV 76-2 planned dive track. B) Side scan sonar map of AUV dive show multiple round depressions. C) Detailed side scan sonar map of AUV dive show multiple round depressions.

188 individuals, 66%/72/%/50% images) and red amphipods (ART_028) (49/450/167 individuals, 31%/54/%/40% images). Further taxa present at the three Vestnesa Ridge OFOBS transects were two morphospecies of eelpouts (CHO_026, CHO_028), pink-coloured amphipods (ART_025), infaunal echiuran annelids (ANN_014), orange-yellow striped large-sized pycnogonids (ART_34), resembling *Colossendeis proboscidea*, buccinid and naticid gastropods (MOL_002_Mol_003, MOL_013), large, white, often partially buried starfish (AST_001) as well as small holothurians of the genus *Elpidia* (HOL_002). Rare and infrequent taxa were stalked Cirripedia (ART_033), stalked crinoids (CRI_001) and anthozoans (CNI_012, CNI_016, CNI_032). In tubeworm forests, indicative of active methane seepage, 22 additional taxa were observed (Table 2), of which most also occurred in close proximity of the worm tube patches. The small buccinoid gastropod (MOL_014) was only seen in tubeworm forests.

The abundance of the ophiuroid (OPH_008) and the occurrence of selected taxa that seem associated with bacterial mat and tubeworm forest covered seafloor were plotted in relation percentage seafloor category for the three OFOBS transects (Figs. 4–7). The displayed percentage seafloor categories were mud (M), coloured sediments (CS), bacterial mats (BM), tubeworm forest alive (WTA), tubeworm forest overgrown (WTD). The ophiuroid (OPH_008) abundance was plotted on top of the percentage seafloor category using the same scale while occurrences of the selected taxa, ranging from none to 14 individuals per images, were plotted individually above. Ophiuroid (OPH_008) abundances were negatively correlated with the presence of bacterial mats, and of live and overgrown tubeworm forests (Figs. 4–6).

On the MSM108 OFOBS transect in 1357 m water depth, ophiuroid numbers ranged from 80 to 150 individuals per images in general areas of mud. Ophiuroid abundance abruptly dropped to zero within the sequence of ten timed images of 100% mud category, which then reduced to include the presence of either bacterial mats or tubeworm forests (Fig. 4A). Taxa like the sabellid polychaete (ANN_003), the red amphipod (ART_028) and the holothurian *Elpidia* sp. (HOL_002) were present in low numbers continuously during the transect (Fig. 4B). The presences of eelpouts (CHO_028), pink amphipods (ART_025) and isopods *Eurycope* sp. (ART_038) seemed associated with the vicinity and presence of bacterial mats and inhabited living tubeworm forests, which are interpreted as a proxy for methane seepage.

On the PS136 OFOBS transect in 1229 m water depth, ophiuroid numbers ranged from 50 to 240 individuals per images in general areas of mud, with most of the images showing more than one hundred ophiuroids (Fig. 5A). Significant drops in ophiuroid numbers, down to complete absence, were recorded in the vicinity of bacterial mat and worm tube patches. Taxa such as sabellid polychaetes (ANN_003), red amphipods (ART_028), and holothurians *Elpidia* sp. (HOL_002) were present throughout the image transect (Fig. 5B). The presence of the eelpout (CHO_028), pink amphipod (ART_025), isopod (ART_38) and the cnidarian (CNI_036) seemed to be positively correlated with the presence of bacterial mats and tubeworm forests. While the cnidarian (CNI_036) was present in singletons in images of living tubeworm forests, its abundance was higher, with up to 40 individuals per image in patches of overgrown tubeworm forests (Fig. 5 B).

On the PS143/1 OFOBS transect in 1282 m water depth, ophiuroid numbers ranged from 30 to 200 individuals per images in general areas of mud, with most of the images showing more than one hundred ophiuroids (Fig. 6). In similarity with the results of the MSM108 and PS136 OFOBS transects, ophiuroid (OPH_008) numbers dropped to zero in vicinity of bacterial mat and tubeworm forests. Taxa such as the sabellid polychaete (ANN_003) and red amphipod (ART_028) were present regularly throughout the image transect, while the presence of holothurian *Elpidia* sp. (HOL_002) was less frequent than observed in the other two transects. The presence of eelpout (CHO-028) and pink amphipod (ART_025) seemed positively correlated with the presence of

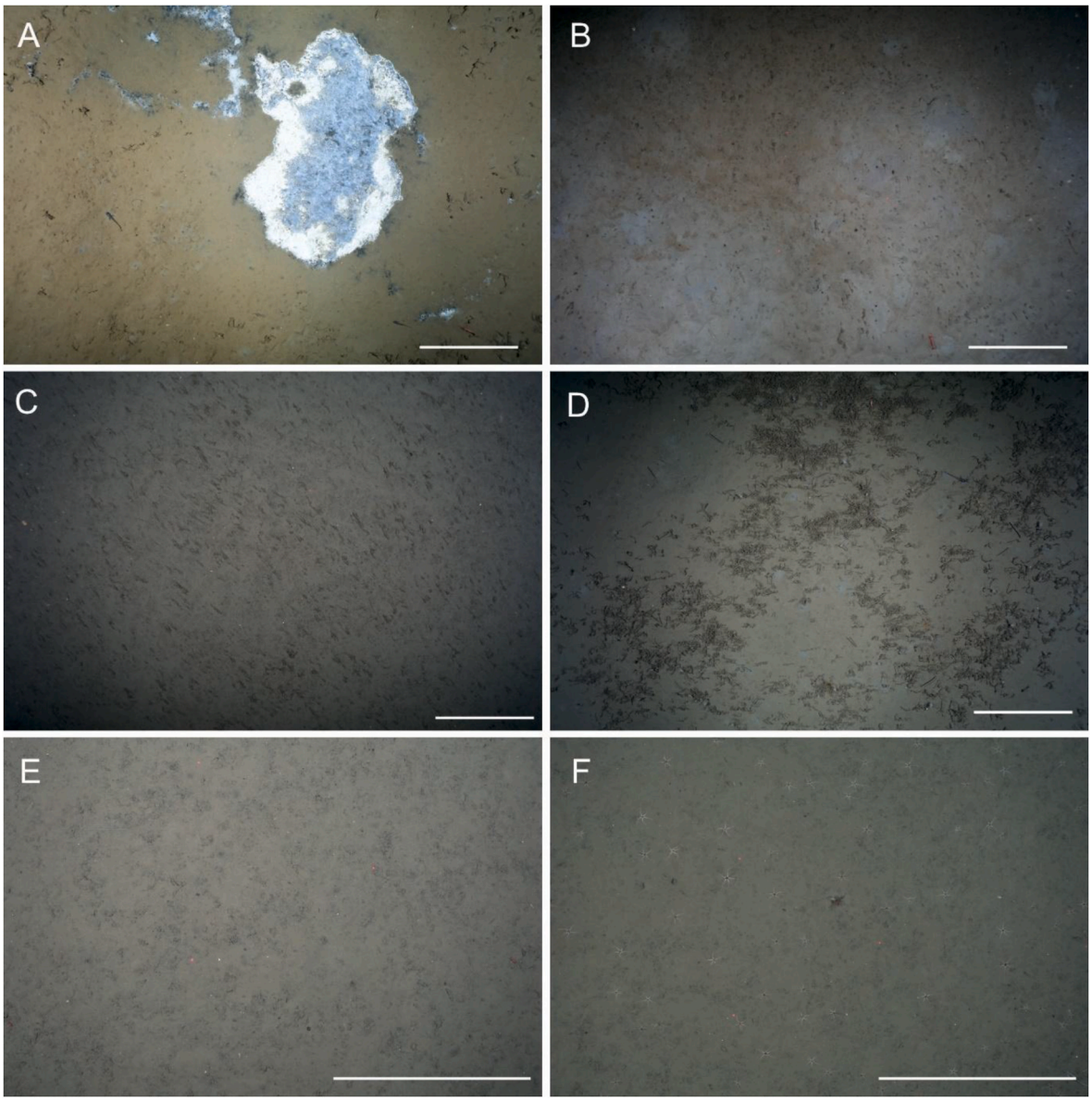

Fig. 3. Seafloor categories. A) Bacterial mats. B) Coloured sediments. C) Tubeworm forest of polychaetes with non-overgrown tubes. D) Tubeworm forest with epifaunal overgrown tubes. E) Seepage influenced mud without ophiuroids. F) In-active mud sediment with phytodetritus layer and ophiuroids. Scale bar 50 cm.

bacterial mats and tubeworm forests. The small gastropod MOL_014 was only present in inhabited tubeworm forests.

The biological images analyses of the three OFOBS stations at the Hœnir methane seep field on the north-western Vestnesa Ridge resulted in the identification of 47 taxa, with 19 taxa present in three OFOBS transects of MSM108/PS136/PS143/1 (Supplement Table 1). Ten of the megafaunal taxa present in the OFOBS images were not listed in the benthic taxon catalogue by Hemmateenejad et al. (2025b). Seventeen of the taxa reported from the OFOBS transect were listed from methane seepage on the Vestnesa Ridge in the benthic taxon catalogue (Hemmateenejad et al., 2025b), followed by 13 shared taxa from methane seepage on Svyatogor Ridge and eight taxa from methane seepage on the Prins Karls Foreland. Taxon sharing with further methane seepage sites in the vicinity of Svalbard was lower, ranging from six taxa shared with the Hakon Mosby Mud Volcano to one species with Kongsfjorden (Table 3).

During PS143/1, benthic fauna from the Vestnesa Ridge Hœnir methane seep field were collected by ROV and EBS (Table 1) and individual specimens were selected for photographs, as representatives of the taxa identified in OFOBS images, and for DNA barcoding (Figs. 7 and 8, Supplement Table 2). Six taxa, comprising two taxa of gastropods (rissoid and buccinoid) and polychaetes (oweniid and sabellid) each, and one taxon of bivalve (yoldiellid) and nemertean (golfingiid) each, were found within bacterial mat samples collected by ROV (Fig. 8).

A total of 95 individuals from 43 taxa were selected for COI barcoding, to confirm systematic positions and to provide genetic barcodes to public molecular sequence databases for future comparisons (Supplement Table 2). Of these, 54 individuals returned valid high quality COI barcodes and their sequences were compared with sequences present in the NCBI BLAST and BIN systems. The NCBI BLAST returned sequence matches of above 70% identity for 42 individuals and in 24 individuals above 95% identity, enabling lower level taxon identification (Supplement Table 2). Species identification with more than 95% identity could only be confirmed for the amphipods *Anonyx nugax, Rhachotropis lomonosovi*, and *Paroediceros propinquus*, the cumacean *Diastylis rathkei,* the decapod *Hymenodora glacialis*, the ophiuroid *Ophiocten gracilis* and the eelpout *Lycenchelys kolthoffi*. For the other sequences, either the percentage of identity or the taxonomic resolution

Table 2
Total abundances and % presence on images of visible taxa in OFOBS images of MSM108, PS136 and PS143/1. Taxa in bold were present in tubeworm forests, taxa marked with * were absent in Hemmateenejad et al. 2025b.

Taxon ID_Code	Phylum	Class/Order	Lowest morphotaxon id	MSM108			PS136			PS143/1		
				Ind.	Image		Ind.	Image		Ind.	Image	
				N	N	%	N	N	%	N	N	%
ANN_003	**Annelida**	**Polychaeta**	**Sabellidae**	179	99	66.9	657	348	72.7	188	133	50.6
ANN_004	Annelida	Polychaeta						16	3.3			
ANN_006	Annelida	Polychaeta					144	5	1.0			
ANN_014	Annelida	Echiura	Bonellidae	6	5	3.4	3	3	0.6	2	2	0.8
ANN_016*	Annelida	Polychaeta	Polynoidae	12	11	7.4	1	1	0.2			
ANN_017*	Annelida	Polychaeta		382	62	41.9						
ART_001	**Arthropoda**	**Decapoda**	**Caridea**							6	3	1.1
ART_008	**Arthropoda**	**Decapoda**	**Caridea**	6	6	4.1	6	4	0.8	8	8	3.0
ART_025	**Arthropoda**	**Amphipoda**		11	9	6.1	46	35	7.3	29	19	7.2
ART_027	**Arthropoda**	**Amphipoda**					55	37	7.7	8	6	2.3
ART_028	**Arthropoda**	**Amphipoda**		49	46	31.1	450	260	54.3	167	107	40.7
ART_033	Arthropoda	Cirripedia	Scalpelomorpha							10	4	1.5
ART_034	Arthropoda	Pycnogonida	*Colossendeis proboscidea sp.*	2	2	1.4	1	1	0.2	3	3	1.1
ART_035	**Arthropoda**	**Pycnogonida**					16	16	3.3	2	2	0.8
ART_036	Arthropoda	Pycnogonida		25	24	16.2	2	2	0.4	4	4	1.5
ART_037*	**Arthropoda**	**Pycnogonida**					1	1	0.2	1	1	0.4
ART_038*	Arthropoda	Isopoda	*Eurycope sp.*	107	35	23.6				68	22	8.4
AST_001	Echinodermata	Asteroidea		5	5	3.4	14	13	2.7	13	11	4.2
AST_003	Echinodermata	Asteroidea		3	3	2.0	4	4	0.8			
AST_020*	**Echinodermata**	**Asteroidea**		1	1	0.7	1	1	0.2			
BRY_006	Bryozoa						3	1	0.2	1	1	0.4
CHO_012	Chordata	Pisces	Rajidae				3	3	0.6	3	3	1.1
CHO_026	Chordata	Pisces	Zoarcidae	3	1	0.7	12	11	2.3	2	2	0.8
CHO_028	**Chordata**	**Pisces**	**Zoarcidae**	10	9	6.1	25	19	4.0	29	22	8.4
CHO_029	Chordata	Pisces	Zoarcidae				1	1	0.2			
CHO_038	Chordata	Pisces		1	1	0.7						
CNI_012	Cnidaria	Anthozoa		2	1	0.7						
CNI_016	**Cnidaria**	**Anthozoa**					3	3	0.6			
CNI_026	Cnidaria	Anthozoa					1	1	0.2			
CNI_032	Cnidaria	Anthozoa										
CNI_036	**Cnidaria**	**Alcyonacea**		1	1	0.7	75	8	1.7	1	1	0.4
CNI_053	**Cnidaria**	**Ceriantharia**	**Cerianthidae**	12	12	8.1	35	31	6.5	13	10	3.8
CRI_001	**Echinodermata**	**Crinoidea**								1	1	0.4
CRI_002	Echinodermata	Crinoidea	Comatulida				1	1	0.2			
HOL_002*	Echinodermata	Holothuroidea	Elpidia sp.	18	15	10.1	116	89	18.6	15	12	4.6
IND_032*	Indet						8	5	1.0	2	1	0.4
MOL_002	**Mollusca**	**Gastropoda**	**Buccinidae**	1	1	0.7	17	14	2.9	2	1	0.4
MOL_003	**Mollusca**	**Gastropoda**	**Buccinidae**	1	1	0.7	7	6	1.3	1	1	0.4
MOL_013	Mollusca	Gastropoda	Naticidae	1	1	0.7	5	5	1.0	2	1	0.4
MOL_014*	**Mollusca**	**Gastropoda**								23	7	2.7
NEM_004	Nemertea			1	1	0.7	5	4	0.8			
OPH_004	**Echinodermata**	**Ophiuroidea**		5	4	2.7	4	4	0.8	2	1	0.4
OPH_008	Echinodermata	Ophiuroidea	Ophiocten sp.	12301	116	78.4	47074	407	85.0	15606	187	71.1
OPH_010	Echinodermata	Ophiuroidea		2	2	1.4						
PLA_001*	Platyhelminthes	Turbellaria		3	3	2.0	4	4	0.8	5	5	1.9
POR_009	Porifera						28	13	2.7	24	5	1.9

was insufficient. In the cases of the amphipods *Rachotropis limosnosovi* and *Anonyx nugax* matching barcodes confirmed the morphological species identification. All Ophiuroid specimens morphologically assigned to *Ophiocten* sp. matched with >99% identity to *Ophiocten gracilis*, showing consistent identity values and BIN clustering.

4. Discussion

The discovery of bacterial mats and dense seep-associated tubeworm forests on the north-western flank of the Vestnesa Ridge gave the first evidence for the existence of active methane seepage on this flank of the ridge. Previous expeditions had reported inactive pockmarks and palaeo-methane seep environments from the area (Ambrose et al., 2015; Consolaro et al., 2018; Ramachandran et al., 2022). The Hœnir seep field is characterised by soft sedimented, muddy non-seep seafloor areas and sporadic, decimeter-sized patches of bacterial mats or tubeworm forests or a combination of both. The bacterial mats did not show visible epifauna on them, whereas ROV samples from these comprised two species of small rissoid and buccinid gastropods, one species each of yoldiid bivalves, golfingiid nemerteans, oweniid and sabellid polychaetes, all representatives of taxa which have been reported from Arctic methane seep and vent fields previously (Åström et al., 2016, 2016, 2020, 2016; Eilertsen et al., 2024). A taxon commonly reported from active Arctic methane seeps, thyasirid bivalves, were not found in the bacterial mats (e.g. Åström et al., 2016; Konovalova et al., 2024). The tubeworm forests defined as alive, often formed by siboglinid polychaetes and oligochaetes in methane seeps (Schulze and Halanych, 2003; Åström et al., 2016), were habitat for seep-associated fauna, which were only seen there or occurred in higher abundances, such as the pink-coloured amphipods (ART_001), pink-coloured caridean shrimp (ART_001), buccinid gastropods (MOL_001, MOL_014), the alcyonarian (CNI_036) and eelpout (CHO_028). Representatives of these seep-associated taxa have been reported from Arctic methane seep and vent fields (e.g. Åström et al., 2016; Eilertsen et al., 2024; Konovalova et al., 2024). Arctic seeps, based on quantitative sampling of macro- and megafauna, have been reported to show relatively higher taxonomic richnesses and abundances than nearby non-seep areas (Carroll et al., 2008; Cochrane et al., 2012; Åström et al., 2020; Konovalova et al.,

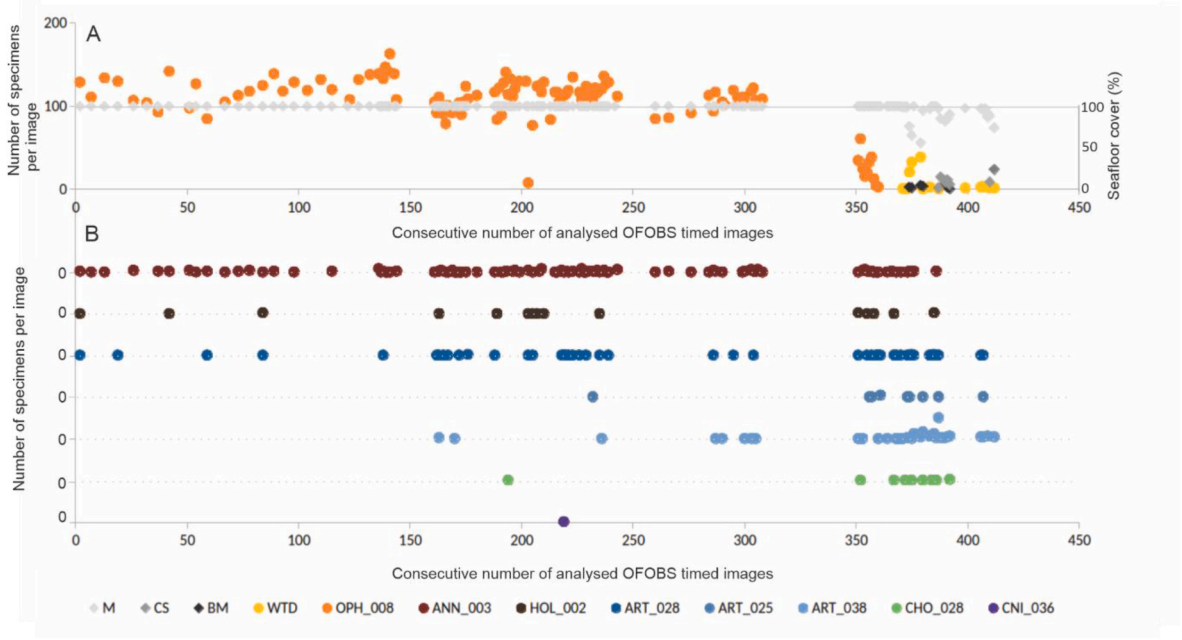

Fig. 4. Seafloor cover and faunal abundances along the OFOBS 7-2 transect station with 187 analysable images of 412 timed images during MSM108. A) Percentage seafloor cover in relation to the abundance of the ophiuroid OPH_008 per analysed image. B) Individual abundance plots of selected taxa, all with <10 specimens per image (for abbreviations see Table 2) Abbreviations: Seafloor cover: BM – bacterial mats. CS – coloured sediments. M – mud. WTA – tubeworm forest with non-overgrown tubes. WTD - tubeworm forest with epifaunal overgrown tubes. Taxon ID codes follow Table 2.

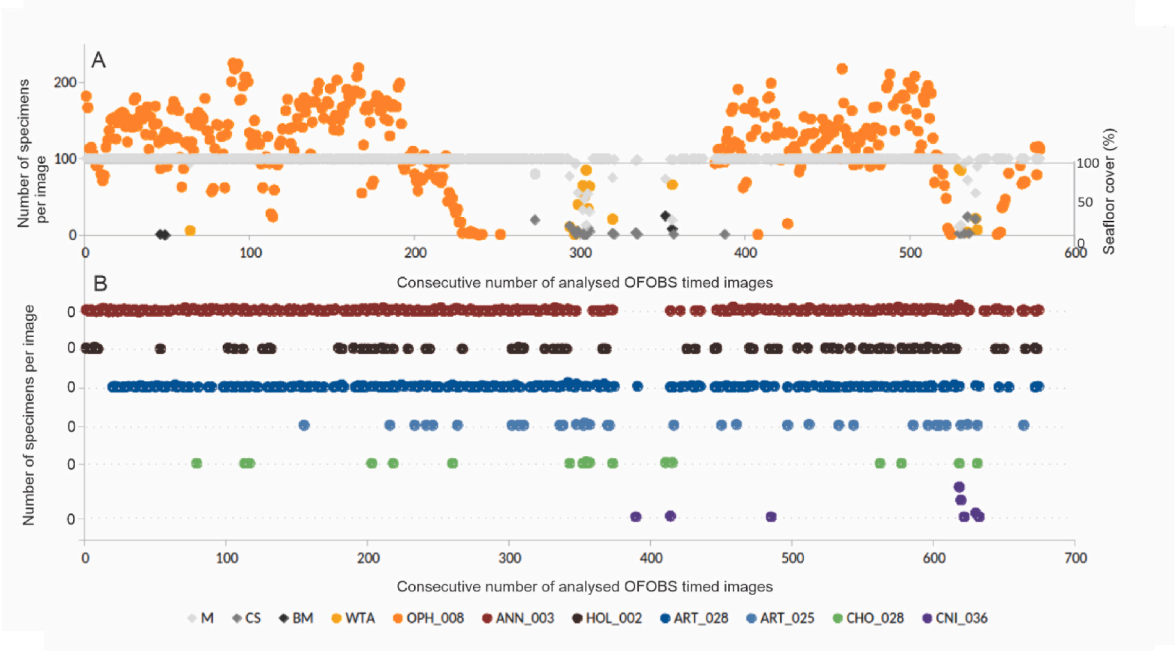

Fig. 5. Seafloor cover and faunal abundances along the OFOBS 22-1 transect with 479 analysable images of 579 timed images during PS136. A) Percentage seafloor cover in relation to the abundance of the ophiuroid OPH_008 per analysed image. B) Individual abundance plots of selected taxa, with <10 specimens per image, apart from CNI_036 with up to 40 specimens per image (for abbreviations see Table 2) Abbreviations: Seafloor cover: BM – bacterial mats. CS – coloured sediments. M – mud. WTA – tubeworm forest with non-overgrown tubes. WTD - tubeworm forest with epifaunal overgrown tubes. Taxon ID codes follow Table 2.

2024). This study analysed in-situ images for megafauna only and therefore the reported taxon diversity per small-scale area, e.g. per image, is likely to be underrepresented. The tubeworm forests in the *Hænir* seep field showed higher abundances and numbers of different species visible per image, but in total the taxa seen in active seepage images were lower than in non-seep images. A halo zone around the active seepage areas was defined by more frequent occurrence of mobile taxa such as skates (CHO_12), eelpouts (CHO_25, CHO_28), pycnogonids (ART_034, ART_035, ART_036), predatory buccinid gastropods (MOL_002) and polynoid polychaetes (ANN_016). The megafauna diversity and composition seen on non-seep soft sediment images from 1200 m to 1400 m depth, dominated by ophiuroids (OPH_008), frequent presence of reddish amphipods of most likely multiple species (ART_025), sabellid polychaetes (ANN_003) and regular occurrences of

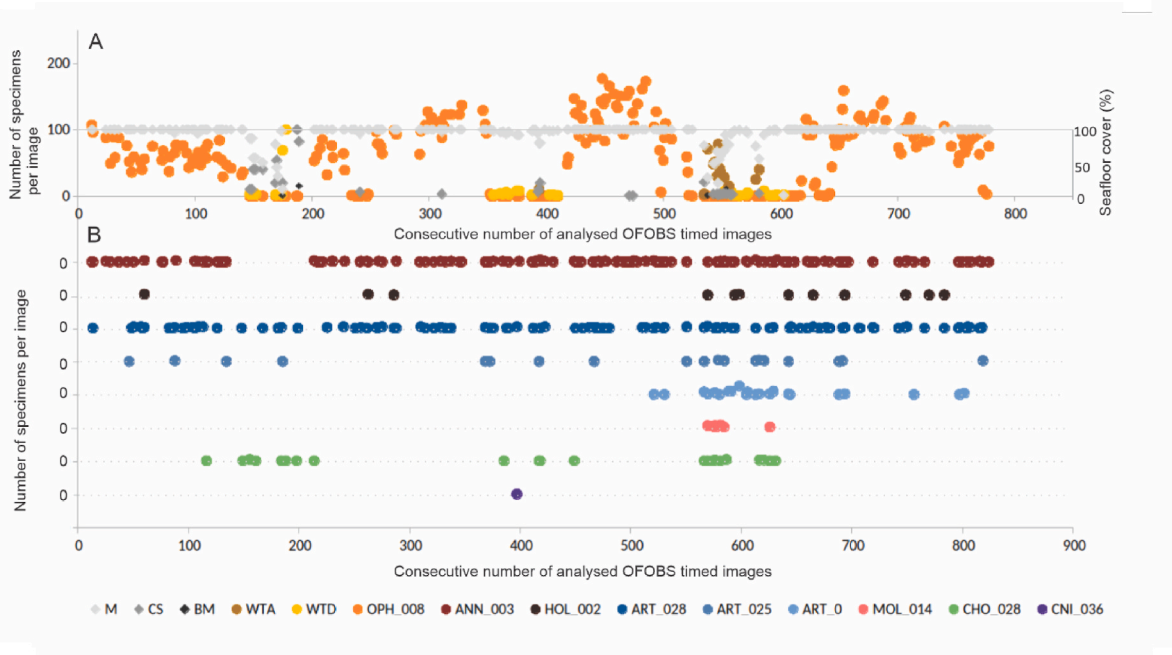

Fig. 6. Seafloor cover and faunal abundances along the OFOBS 23-2 transect with 263 analysable images of 841 timed images during PS143/1. A) Percentage seafloor cover in relation to the abundance of the ophiuroid OPH_008 per analysed image. B) Individual abundance plots of selected taxa, with <10 specimens per image (for abbreviations see Table 2) Abbreviations: Seafloor cover: BM – bacterial mats. CS – coloured sediments. M – mud. WTA – tubeworm forest with non-overgrown tubes. WTD - tubeworm forest with epifaunal overgrown tubes. Taxon ID codes follow Table 2.

small *Elpidia* sp. holothurians (HOL_002), differ from the megafauna composition described from the HAUSGARTEN stations N3, HG-IV and S3 at 2300 m to 2800 m depths (Taylor et al., 2016; 2017). At these deeper stations a total of 27 taxa were recorded, and in contrast to the non-seep areas in the *Hœnir* seep field, ophiuroids were absent, as well as the presence of the poriferans *Caulophacus arcticus* and *Cladorhiza* cf. *gelida*, the holothurian *Kolga hyalina*, and the asteroid *Hymenaster pellucidus* (Taylor et al., 2017). Faunal elements such as the holothurian *Elpidia* sp. and the stalked crinoid *Bathycrinus* sp. were recorded at all sites, but their abundances and frequencies were higher in depths deeper than 2000 m. Studies on the macrobenthic fauna of the deep Fram Strait using a box corer have included the HAUSGARTEN station HG-I, in close proximity with the OFOBS transects analysed here (Käß et al., 2019). Here, polychaetes with ~45% relative abundance have been reported as the most abundant taxon, followed by molluscs (~20%) and crustaceans (~20%). Echinoderms were grouped in "Others" with less than 5% relative abundance. Comparing the relative abundance results of this study with those of Käß et al. (2019) showed clear differences between mega- and macrofaunal relative abundances.

The megafaunal assemblage in the active areas of the *Hœnir* methane seep field comprised 22 taxa adjacent to the tube forming annelids and resembled the megafaunal taxa observed in methane seep environments around Svalbard (Åström et al., 2016, 2018, 2019, 2020; Eilertsen et al., 2025). Detailed studies on Arctic methane seep diversity have included quantitative sampling for infaunal and macrofaunal taxa. These studies reported higher taxon numbers and collected physical specimens for identification, enabling species identification (Åström et al., 2016, 2018, 2019, 2020; Konovalova et al., 2024; Eilertsen et al., 2025). A comparable study from the *Hœnir* methane seep field is underway. An EBS was trawled during PS143/1, within and across the methane seep field but the macrofauna collected and hand-picked for COI barcoding comprised specimens from both within and outside of active seepage areas, integrated into one sample by the sampling methodology. Using the COI barcode sequences from selected hand-picked specimens for species identification via the NCBI BLAST and BIN systems showed the knowledge gap for barcode sequences in deep-sea Arctic and northern North Atlantic benthos. Given the low coverage of the identified species in publicly available datasets, genetic barcoding in such extreme habitats provides a valuable source of information and may support future taxonomic, ecological, and biogeographic studies.

Analyses of deep-sea in-situ images, particularly those taken by towed camera systems, have their limitations regarding high individual error, inter-observer variability, incorrect faunal identifications and quantitative abundances calculations (e.g. Durden et al., 2016; Taylor et al., 2016; Horton et al., 2021). In this study, the same observer annotated all images and cross-checked faunal identifications between transects of different expeditions and within transects, as well as excluding images of insufficient quality from the analyses. The best practise of open nomenclature signs for taxon identification and morphospecies identification recommended by Horton et al. (2021) was used. To support faunal comparisons with morphospecies reported from other Arctic methane seep sites, the taxon codes established by Hemmateenejad et al. (2025b) were used and extended if taxa were reported that were absent in the latter catalogue. This study analysed seafloor category and faunal assemblages in a descriptive qualitative way as we were aware of the potential limitation due to the influence of spatial variation of biota and habitat features (Taylor et al., 2017). Because of technical and ship time constraints this study is based on *in-situ* images taken from a single OFOBS transect at each station during the three expeditions, following similar approaches taken by Taylor et al. (2016, 2017), Teixidó et al. (2004, 2007) and MacDonald et al. (2010). Clearly, the AUV, OFOBS and ship bathymetry from the region indicate the locally high heterogeneity of fauna are associated with an at least partially active region of the western Vestnesa Ridge with an approximate diameter of 3 – 500 m and linear extent (WNW to ESE trend) on potentially 10s of kilometers (Fig. 2). Our discovery of the Hœnir seep field on the western flank of the Vestnesa Ridge shows that the current knowledge on the presence and distribution of active methane seeps in the vicinity of Svalbard is incomplete. The Vestnesa Ridge, despite being one of the best studied areas in the Arctic regarding past and recent methane seeps (e.g. Bünz et al., 2012; Ambrose et al., 2015; Panieri et al., 2017; Consolaro et al., 2018: Schneider et al., 2018; Åström et al.,

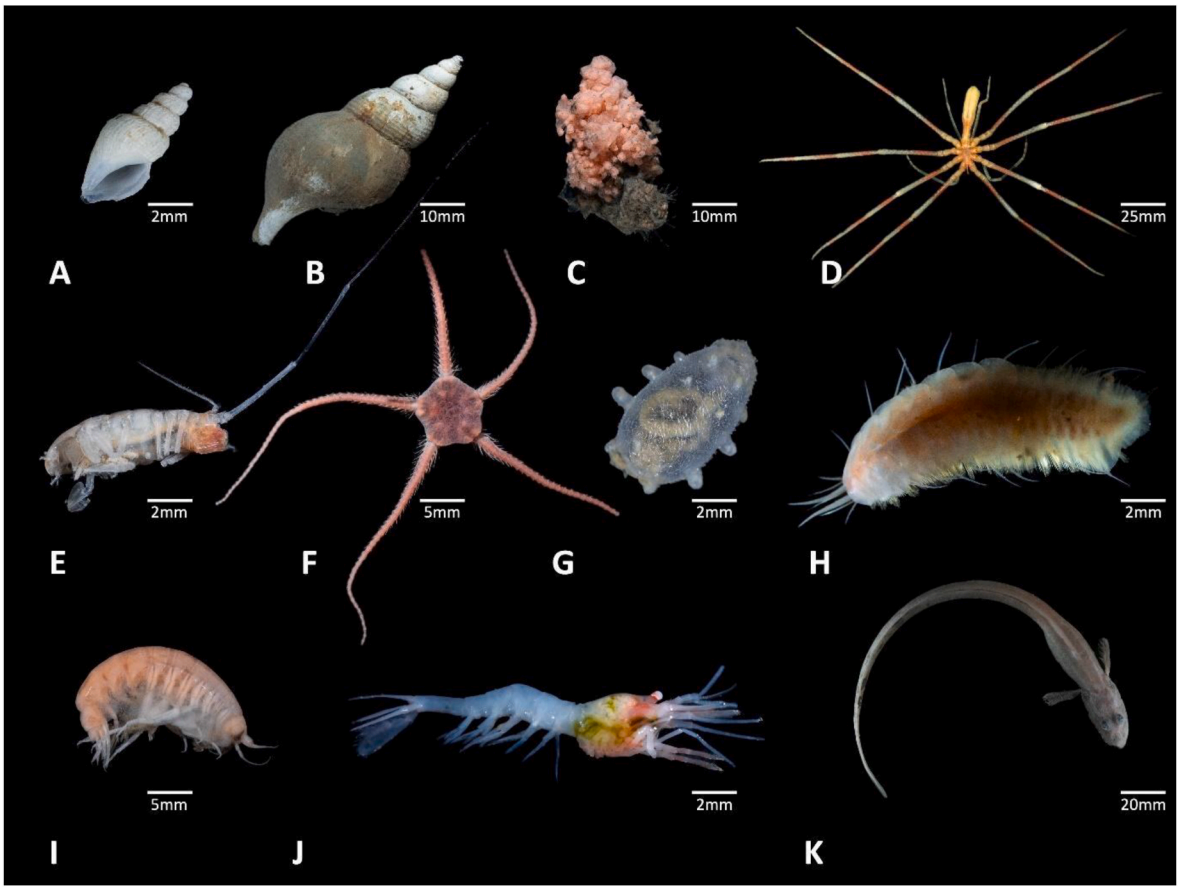

Fig. 7. Representative morphospecies of the taxon code given fauna of the OFOBS image analyses. Taxon names of the photographed specimens, with resemble the coded taxon appear in brackets. A) MOL_003 (Buccinidae). B) MOL_002 (Buccinidae). C) CNI_036 (Alcyonacea). D) ART_034 (*Colossendeis proboscidea* sp.). E) ART_038 (*Eurycope* sp.). F) OPH_008 (*Ophiocten* sp.). G) HOL_002 (*Elpidia* sp.). H) ANN_016 (Polynoidae). I) ART_028 (Amphipoda). J) ART_008 (Caridea). K) CHO_028 (Zoarcidae). For each specimen a scale is given in mm.

Table 3
Taxon numbers at this studies' Vestnesa Ridge OFOBS transects and shared taxa at Arctic and Barent Sea methane seepage sites following Hemmateenejad et al. (2025b).

Phylum	Class/Order	this study	VR	7808	SvR	PKF	KF	Sfr	HT	HMMV	VSl
Annelida	Polychaeta	5	3		3	1		1	1		
Annelida	Echiura	1									
Arthropoda	Decapoda	2	1		2						
Arthropoda	Amphipoda	3	1		3						
Arthropoda	Cirripedia	1	1								
Arthropoda	Pycnogonida	4	2			3	1	1	1	2	2
Arthropoda	Isopoda	1									
Echinodermata	Asteroidea	3	1		1	1		1	1	1	1
Bryozoa		1									
Chordata	Pisces	6	2	1	1				1	2	1
Cnidaria	Anthozoa	4	1	1	2						
Cnidaria	Alcyonacea	1	1			1		1			
Cnidaria	Ceriantharia	1	1								
Echinodermata	Crinoidea	2			1	1					
Echinodermata	Holothuroidea	1									
Indet.		1									
Mollusca	Gastropoda	4	1	1	2	1		2		1	1
Nemertea		1	1								
Echinodermata	Ophiuroidea	3	2	1	1						
Plathelminthes		1									
Porifera		1			1	1					
	Shared taxa	47	**18**	**4**	**17**	**9**	**1**	**6**	**4**	**6**	**5**

Abbreviations: HMMV – Hakon Mosby Mud Volcano, HT – Hinlopen Trough,KF – Kongsfjorden, PKF – Prins Karl Foreland, Sfr – Storfjordrenna, SvR – Svyatogor Ridge, VR – Vestnesa Ridge, VSl – Vestbakken Slope, 7808 – Site 7808

2019; Rasmussen and Nielsen, 2024), hosts active methane seep fields at different water depths and that these discreet seep fields comprise contrasting faunal assemblages. The faunal taxa recorded from the Hœnir seep field show biogeographic relationships to taxa recorded from

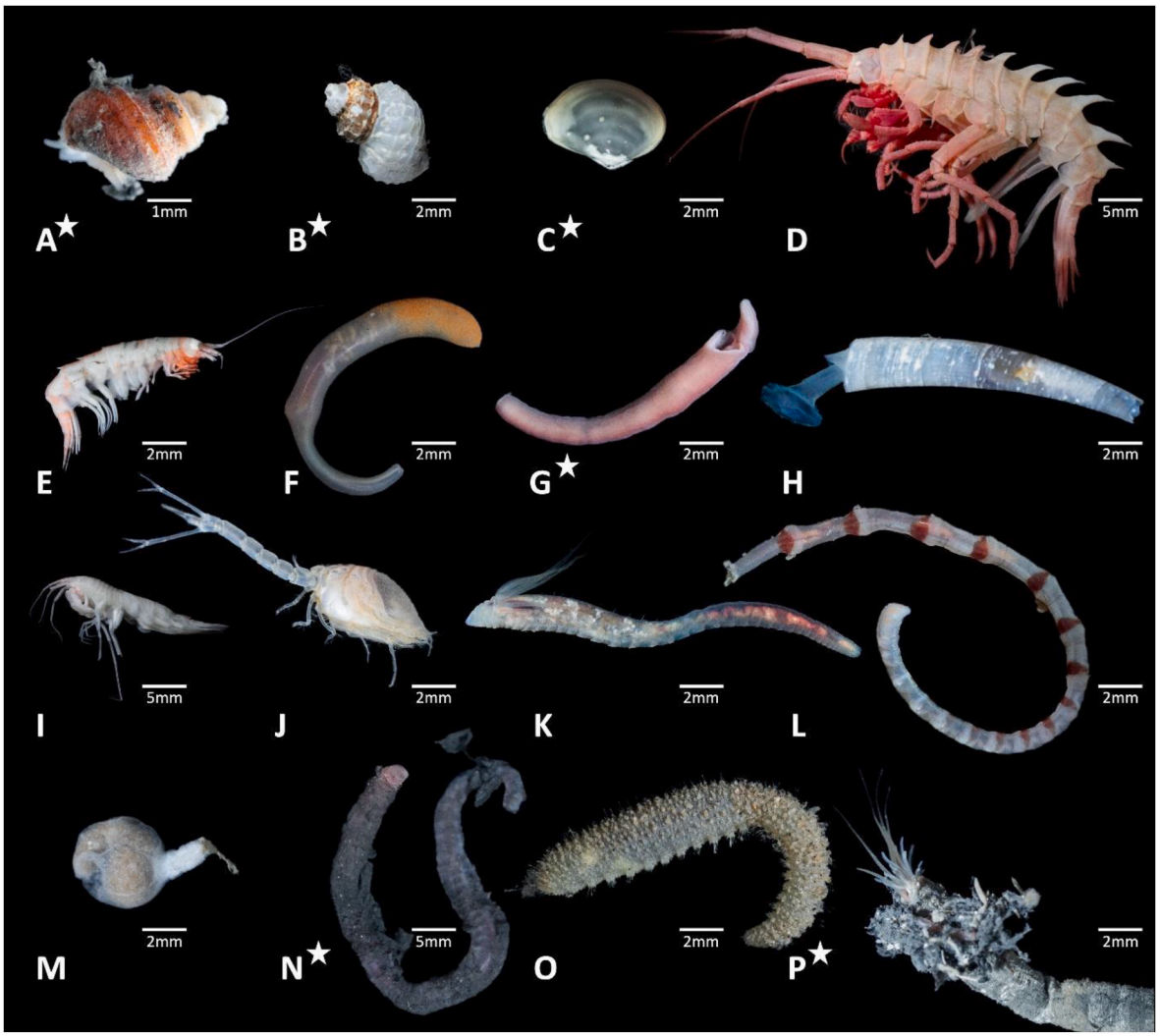

Fig. 8. Representatives of benthic fauna collected in the methane seepage area by EBS and ROV. A) Gastropod sp. A* (HG540). B) Gastropod sp. B* (HG389). C) *Yoldiella* sp.* (HG544). D) *Amathillopsis spinigera* (HG510). E) *Hallirages aff. qvadidentatus* (HG436). F) *Nephasoma* sp. (HG534). G) Nemertea sp.* (HG535). H) Scaphopoda sp. (HG271). I) *Rachotropis lomonosovi* (HG424), J) *Diastylis polaris* (HG331). K) Ampharetidae sp. (HG258). L) Maldanidae sp. (HG336). M) *Lucernaria* sp. (HG451), N) Owenidae sp.* (HG539). O) *Brada* sp. (HG253). P) Sabellidae sp.* (HG538). Specimens associated with the bacterial mats are marked with a white star. For each specimen a scale is given in mm. In brackets the expedition sample ID is given.

other Arctic seep and vent fields, but these need to be confirmed by molecular genetic comparisons to understand faunal connectivity and evolutionary radiation processes between the fauna of the Arctic hydrothermal ecosystems.

CRediT authorship contribution statement

Katrin Linse: Writing – original draft, Visualization, Investigation, Formal analysis, Data curation, Conceptualization. **Lilian Boehringer:** Visualization, Investigation, Formal analysis, Data curation. **Saskia Brix:** Writing – review & editing, Resources, Investigation, Funding acquisition, Data curation. **Jennifer Dannheim:** Writing – review & editing, Supervision. **Jonas Hagemann:** Investigation, Data curation. **Fereshteh Hemmateenejad:** Methodology. **Áki Jarl Láruson:** Writing – review & editing, Supervision, Investigation, Formal analysis. **Giuliana Panieri:** Writing – review & editing, Validation, Supervision, Methodology. **Lydia Anastasia Schmidt:** Visualization, Investigation. **Maximilian Schrade:** Data curation, Formal analysis, Investigation, Visualization. **Carolin Uhlir:** Investigation. **Autun Purser:** Writing – review & editing, Methodology, Investigation, Data curation, Conceptualization.

Declaration of competing interest

The authors declare that they have no known competing financial interests or personal relationships that could have appeared to influence the work reported in this paper.

Acknowledgements

We thank captains Thomas Wunderlich and Felix Lauber and their crews for their support during PS136 and PS143/1-1. KL, SB, AJL, LAS, and CU are grateful to PSOs Thomas Soltwedel and Frank Wenzhöfer for their invite to participate in the expeditions as part of the AWI Deep Sea group, for the ship time to deploy the EBS and especially for the opportunity of the ROV Kiel 6000 dive at the Hœnir methane seep field. We

sincerely thank Karen Jeskulke for the technical and molecular support and database management. We are grateful to two anonymous reviewers for their constructive comments that improved the earlier manuscript versions.

This study was supported by grant no. AWI_PS136_01 and AWI_PS143/1_1. KL is funded by BIOPOLE under the Natural Environment Research Council National Capability Science Multi-Centre award scheme (NC-SM2). LB is funded by AWI INSPIRES-III. SB and CU received support via the Leibniz foundation and the ALONGate project (A Long-term Observatory of the North Atlantic Gateway to the Arctic Ocean) via grant number PS150/2023 in the program for women professors. MS is funded by the Biodiverse Anthropocene Progamme (ANTS) and the Finnish Cultural Foundation.

This paper contributes to the BIOPOLE, IceAGE, ALONGate and HAUSGARTEN programmes.

This publication (#003-25) includes molecular data generated with the support of the LIB – Center for Molecular Biodiversity Research's Molecular Laboratory in Hamburg.

Supplement Tables.

Supplement Table 1

ID_Code	Phylum	Class/Order	MSM108	VR-PS136	VR-PS143/1	VR	7808	SvR	PKF	KF	Sfr	HT	HMMV	VSl
ANN_003	Annelida	Polychaeta	x	x	x	x								
ANN_004	Annelida	Polychaeta	x	x		x		x	x		x	x		
ANN_006	Annelida	Polychaeta		x		x		x						
ANN_014	Annelida	Echiura	x	x	x									
ANN_016	Annelida	Polychaeta	x	x	x									
ANN_017	Annelida	Polychaeta	x											
ART_001	Arthropoda	Decapoda			x	x		x						
ART_008	Arthropoda	Decapoda	x	x	x			x						
ART_025	Arthropoda	Amphipoda	x	x	x	x		x						
ART_027	Arthropoda	Amphipoda		x	x			x						
ART_028	Arthropoda	Amphipoda	x	x	x			x						
ART_033	Arthropoda	Cirripedia			x	x								
ART_034	Arthropoda	Pycnogonida	x	x	x	x			x		x		x	x
ART_035	Arthropoda	Pycnogonida		x	x	x			x			x	x	x
ART_036	Arthropoda	Pycnogonida	x	x	x				x	x				
ART_037	Arthropoda	Pycnogonida		x	x									
ART_038	Arthropoda	Isopoda	x		x									
AST_001	Echinodermata	Asteroidea	x	x	x	x		x					x	x
AST_003	Echinodermata	Asteroidea	x	x					x		x	x		
AST_020	Echinodermata	Asteroidea	x	x										
BRY_006	Bryozoa			x	x									
CHO_012	Chordata	Pisces		x	x	x		x				x	x	x
CHO_026	Chordata	Pisces	x	x	x			x						
CHO_028	Chordata	Pisces	x	x	x	x							x	
CHO_029	Chordata	Pisces		x			x							
CHO_038	Chordata	Pisces	x											
CNI_012	Cnidaria	Anthozoa	x											
CNI_016	Cnidaria	Anthozoa		x	x			x						
CNI_026	Cnidaria	Anthozoa		x		x	x							
CNI_032	Cnidaria	Anthozoa			x			x						
CNI_036	Cnidaria	Alcyonacea	x	x	x	x			x		x			
CNI_053	Cnidaria	Ceriantharia	x	x	x	x								
CRI_001	Echinodermata	Crinoidea			x			x						
CRI_002	Echinodermata	Crinoidea		x					x					
HOL_02	Echinodermata	Holothuroidea	x	x	x									
IND_032	Indet			x	x									
MOL_002	Mollusca	Gastropoda	x	x		x		x			x		x	
MOL_003	Mollusca	Gastropoda	x	x			x	x	x		x			x
MOL_013	Mollusca	Gastropoda	x	x										
MOL_014	Mollusca	Gastropoda			x									
NEM_004	Nemertea		x	x		x								
OPH_004	Echinodermata	Ophiuroidea	x	x	x	x	x							
OPH_008	Echinodermata	Ophiuroidea		x		x		x						
OPH_010	Echinodermata	Ophiuroidea	x											
PLA_001	Platyhelminthes	Turbellaria	x	x	x									
POR_009	Porifera			x	x			x	x					
		Shared taxa	28	36	30	**18**	**4**	**17**	**9**	**1**	**6**	**4**	**6**	**5**

Supplement Table 2

Phylum	Class	Order	Family	Genus - Morph ID	Species - Morph ID	N	Expedition Sample ID	BoLD Process ID	NCBI % Identity	NCBI Match ID	NCBI sequence ID	BIN Match ID	BIN Sequence ID
Annelida	Polychaeta		**Capitellidae**	***Notomastus***	**sp.**	3	**HG254**	**HGMS023–25**	**99.5**	**Stegocephalidae**	MG264754.1		
				Notomastus	sp.		HG255						
				Notomastus	sp.		HG256						
			Opheliidae	*Ophelina*	*opisthobranchiata*	2	HG260	HGMS025-25	82.33	Polychaeta sp.	KJ736380.1		
				Ophelina	*opisthobranchiata*		HG262	HGMS027-25	82.1	Polychaeta sp.	KJ736380.1	*Ophelina cylindricaudata*	BOLD: ACA1257
				Ophelina	*cylindricaudata*	1	HG259	HGMS024-25	83.25	Polychaeta sp.	KJ736380.1		
				Ophelia	sp.	1	HG444	HGMS007-25	82.02	Polychaeta sp.	KJ736380.1	*Ophelina cylindricaudata*	BOLD: ACA1257
		Eunicida	Lumbrineridae		sp.	1	HG264	HGMS028-25	80.42	Lumbrineris sp.	MZ504206.1		
		Terebellida	Flabelligeridae	*Brada*	cf. *tzertlini*	1	HG253	HGMS022-25	85.69	Brada sp.	HQ326970.1		BOLD: ACN1555
		Terebellida	Ampharetidae		sp.	1	HG258						
		Terebellida	Ampharetidae	cf. *Amphicteis*	sp.	1	HG449						
			Scalibregmatidae	*Pseudoscalibregma*	*parvum*	2	HG251	HGMS020-25	81.27	Scalibregmatidae sp.	OP702879.1	Scalibregmatidae	BOLD: ACI8330
				Pseudoscalibregma	*parvum*		HG333	HGMS050-25	81.62	Scalibregmatidae sp.	OP702879.1	Scalibregmatidae	BOLD: ACI8330
			Maldanidae		sp.	3	HG311						
			Maldanidae		sp.		HG336						
			Maldanidae		sp.		HG252						
		Spionida	Spionidae		sp.	1	HG317						
		Sabellida	Sabellidae		sp.	1	HG358						
			Oweniidae		sp.	1	HG539						
		Phragmophora	Heterokrohniidae		sp.	1	HG447						
		Phyllodocida	Phyllodocidae		sp.	1	HG340	HGMS052-25	81.91	*Phyllodoce medipapillata*	OQ626345.1		
			Paraonidae	*Aricidea*	*abranchiata*	1	HG318						
		Sabellida	Siboglinidae		sp.	2	HG440						
			Siboglinidae		sp.		HG441	HGMS006-25	87.52	Ampharetidae sp.	OQ738508.1	Terebellidae	BOLD: AGR6325
	Polychaeta				sp.	1	HG536						
	Polychaeta				sp.	1	HG543						
	Polychaeta				sp.	1	HG448						
	Polychaeta				sp.	1	HG265						
	Polychaeta				sp.	1	HG266						
		Sipuncula	Golfingiidae	*Nephasoma*	*lilljeborgi*	1	HG261	HGMS026-25	74.38	Glycera sp.	MZ504181.1		
		Sipuncula	Golfingiidae	*Nephasoma*	sp.	2	HG534						
				Nephasoma	sp.		HG446	HGMS008-25	74.65	Glycera sp.	MZ504181.1	*Nephasoma lilljeborgi*	BOLD: ACP2517
Arthropoda	Malacostraca	Amphipoda	**Stegocephalidae**		**sp.**	1	**HG294**	**HGMS034–25**	**99.69**	**Stegocephalidae**	MG264754.1	Stegocephalidae	BOLD: ADH9760
		Amphipoda	Eurisidae	*Rhachotropis*	cf. *lomonosovi*	3	HG367						
				Rhachotropis	**cf. *lomonosovi***		**HG424**	**HGMS058–25**	**99.17**	***Rhachotropis lomonosovi***	MG521156.1		
				Rhachotropis	cf. *lomonosovi*		HG429						
		Amphipoda	**Eurisidae**		**sp.**	1	**HG432**	**HGMS059–25**	**100**	***Paroediceros propinquus***	MG264825.1		
		Amphipoda	Uristidae	*Anonyx*	cf. *nugax*	3	**HG382**	**HGMS055–25**	**99.85**	***Anonyx nugax***	MG264780.1		
				Anonyx	cf. *nugax*		**HG383**	**HGMS056–25**	**100**	***Anonyx nugax***	MG264780.1		
				Anonyx	cf. *nugax*		**HG435**	**HGMS003–25**	**99.7**	***Anonyx nugax***	MG264780.1	*Anonyx nugax*	BOLD: AAA9156
		Amphipoda	Pardaliscidae		sp.	1	HG418	HGMS057-25	80.23	Lysianassoidea sp.	KP713916.1		
		Amphipoda	**Eusiroidea**		**sp.**	1	**HG425**	**HGMS059–25**	**100**	***Paroediceros propinquus***	MG264825.1		

(*continued on next page*)

Supplement Table 2 (*continued*)

Phylum	Class	Order	Family	Genus - Morph ID	Species - Morph ID	N	Expedition Sample ID	BoLD Process ID	NCBI % Identity	NCBI Match ID	NCBI sequence ID	BIN Match ID	BIN Sequence ID
		Amphipoda	Ampeliscidae	*Haploops*	*setosa*	2	HG431						
				Haploops	*setosa*		HG300	HGMS035-25	93.17	*Haploops carinata*	OQ053034.1	*Haploops setosa*	BOLD: ACW6741
		Amphipoda	Calliopiidae	*Halirages*	*aff. qvadridentatus B*	2	HG436						
				Halirages	*aff. qvadridentatus B*		HG437						
		Amphipoda	Amathillopsidae	*Amathillopsis*	cf. *spinigera*	9	HG500	HGMS073-25	80.4	*Eusirus* cf. *giganteus*	MT985584.1	*Amathillopsis spinigera*	BOLD: AAR3656
				Amathillopsis	cf. *spinigera*		HG501	HGMS074-25	80.39	*Eusirus* cf. *giganteus*	MT985584.1	*Amathillopsis spinigera*	BOLD: AAR3656
				Amathillopsis	cf. *spinigera*		HG502						
				Amathillopsis	cf. *spinigera*		HG505						
				Amathillopsis	cf. *spinigera*		HG506	HGMS075-25	80.44	*Eusirus* cf. *giganteus*	MT985584.1	*Amathillopsis spinigera*	BOLD: AAR3656
				Amathillopsis	cf. *spinigera*		HG507	HGMS076-25	80.28	*Eusirus* cf. *giganteus*	MT985584.1	*Amathillopsis spinigera*	BOLD: AAR3656
				Amathillopsis	cf. *spinigera*		HG515	HGMS078-25	80.24	*Eusirus* cf. *giganteus*	MT985584.1	*Amathillopsis spinigera*	BOLD: AAR3656
				Amathillopsis	cf. *spinigera*		HG516	HGMS079-25	80.24	*Eusirus* cf. *giganteus*	MT985584.1	*Amathillopsis spinigera*	BOLD: AAR3656
				Amathillopsis	cf. *spinigera*		HG518						
		Amphipoda	Phoxocephalidae	*Harpinia*	cf. *abyssi*	1	HG438	HGMS005-25	79.3	Amphipoda sp.	KP713942.1	*Harpinia abyssi*	BOLD: ACM1288
		Cumacea	Diastylidae	*Diastylis*	Diastylis oxyrhyncha	2	HG452						
				Diastylis	**Diastylis oxyrhyncha**		**HG454**	**HGMS011–25**	**99.84**	***Diastylis rathkei***	MK757524.1	*Diastylis rathkei*	BOLD: AAY6478
		Cumacea	Diastylidae	*Diastylis*	*polaris*	1	HG453						
		Cumacea	Diastylidae	*Diastylis*	*glabra*	1	HG328						
		Decapoda	Acanthephyridae	***Hymenodora***	***glacialis***	2	**HG304**	**HGMS037–25**	**100**	***Hymenodora glacialis***	FJ602519.1	*Hymenodora glacialis*	BOLD: AAF3803
				Hymenodora	***glacialis***		**HG305**	**HGMS038–25**	**99.09**	***Hymenodora glacialis***	FJ602519.1	*Hymenodora glacialis*	BOLD: AAF3803
		Tanaidacea			sp.	2	HG337						
		Tanaidacea			sp.		HG339						
	Pycnogonida	Pantopoda	Colossendeidae	*Colossendeis*	*proboscidea*	1	HG526						
Chaetognatha					**sp.**	1	**HG312**	**HGMS041–25**	**98.49**	**Heterokrohnia sp.**	FJ602474.1	Heterokrohnia sp.	BOLD: AAM9474
Cnidaria	Anthozoa	Actiniaria	Amphianthus		sp.	2	HG482						
			Amphianthus		sp.		HG584						
Chordata	Actinopterygii	Scorpaeniformes	Zoarcidae	***Lycodonus***	***flagellicauda***	1	**HG347**	**HGMS053–25**	**95.13**	***Lycenchelys kolthoffi***	LC493919.1		
Echinodermata	Ophiuroidea	Ophiurida	Ophiuridae	*Ophiocten*	sp.	24	**HG290**	**HGMS031–25**	**99.18**	***Ophiocten gracilis***	KU895451.1		
				Ophiocten	sp.		**HG291**	**HGMS032–25**	**99.56**	***Ophiocten gracilis***	KU895451.1		
				Ophiocten	sp.		**HG293**	**HGMS033–25**	**99.56**	***Ophiocten gracilis***	KU895451.1		
				Ophiocten	sp.		**HG302**	**HGMS036–25**	**99.56**	***Ophiocten gracilis***	KU895451.1		
				Ophiocten	sp.		**HG309**	**HGMS039–25**	**99.71**	***Ophiocten gracilis***	KU895451.1		
				Ophiocten	sp.		**HG319**	**HGMS042–25**	**99.34**	***Ophiocten gracilis***	KU895451.1		
				Ophiocten	sp.		**HG320**	**HGMS043–25**	**99.41**	***Ophiocten gracilis***	KU895451.1		
				Ophiocten	sp.		**HG321**	**HGMS044–27**	**98.98**	***Ophiocten gracilis***	KU895451.1		
				Ophiocten	sp.		**HG322**	**HGMS045–25**	**100**	***Ophiocten gracilis***	PP595071.1		
				Ophiocten	sp.		**HG323**	**HGMS046–25**	**99.56**	***Ophiocten gracilis***	KU895451.1		
				Ophiocten	sp.		**HG324**	**HGMS047–25**	**99.71**	***Ophiocten gracilis***	KU895451.1		

(*continued on next page*)

Supplement Table 2 (*continued*)

Phylum	Class	Order	Family	Genus - Morph ID	Species - Morph ID	N	Expedition Sample ID	BoLD Process ID	NCBI % Identity	NCBI Match ID	NCBI sequence ID	BIN Match ID	BIN Sequence ID
				Ophiocten	sp.		**HG325**	**HGMS048–31**	**99.26**	***Ophiocten gracilis***	KU895451.1		
				Ophiocten	sp.		**HG459**	**HGMS012–25**	**99.27**	***Ophiocten gracilis***	KU895451.1		
				Ophiocten	sp.		**HG460**	**HGMS013–25**	**99.71**	***Ophiocten gracilis***	KU895451.1		
				Ophiocten	sp.		**HG463**	**HGMS014–25**	**99.56**	***Ophiocten gracilis***	KU895451.1		
				Ophiocten	sp.		**HG466**	**HGMS060–25**	**99.71**	***Ophiocten gracilis***	KU895451.1		
				Ophiocten	sp.		**HG530**	**HGMS063–25**	**99.12**	***Ophiocten gracilis***	KU895451.1		
				Ophiocten	sp.		**HG550**	**HGMS065–25**	**99.27**	***Ophiocten gracilis***	KU895451.1		
				Ophiocten	sp.		**HG551**	**HGMS066–25**	**99.41**	***Ophiocten gracilis***	KU895451.1		
				Ophiocten	sp.		**HG552**	**HGMS067–25**	**99.13**	***Ophiocten gracilis***	KU895451.1		
				Ophiocten	sp.		**HG553**	**HGMS068–25**	**99.7**	***Ophiocten gracilis***	KU895451.1		
				Ophiocten	sp.		HG554						
				Ophiocten	sp.		HG557						
				Ophiocten	sp.		HG562						
	Nemertea				sp.	1	HG535						
Nemertini Platyhelminthes					sp.	1	HG528						

Data availability

The EM122, OFOBS and AUV data resulting from the AWI lead expeditions MSM95, MSM108, PS136 and PS143/1are deposited in PANGAEA and dois are referenced in the publication. The data from the image analyses of this study are deposited at the UK Polar Data Centre (Linse et al., 2026). GenBank accession numbers and/or NoLD number for DNA sequences are provided via the BOLD project entitled **Barcoding of benthic marine invertebrates found within the Fram Strait methane seep**, project code **HGMS** (**HausGarten Methane Seep**).

References

Altschul, S.F., Gish, W., Miller, W., Myers, E.W., Lipman, D.J., 1990. Basic local alignment search tool. J. Mol. Biol. 215, 403–410.

Ambrose Jr., W.G., Panieri, G., Schneider, A., Plaza-Faverola, A., Carroll, M.L., Åström, E.K.L., Locke, W.L., Carroll, J., 2015. Bivalve shell horizons in seafloor pockmarks of the last glacial-interglacial transition: a thousand years of methane emissions in the Arctic Ocean. G-cubed 16, 4108–4129. https://doi.org/10.1002/2015GC005980.

Argentino, C., Borrelli, C., Akinselure, A., Correa-Diaz, M., Panieri, G., 2024. Biogeochemical investigations of methane seepage at the ultraslow-spreading arctic mid-ocean ridge: Svyatogor ridge, fram strait. Mar. Petrol. Geol. 162, 106761. https://doi.org/10.1016/j.marpetgeo.2024.106761.

Åström, E.K., Carroll, M.L., Ambrose Jr., W.G., Carroll, J., 2016. Arctic cold seeps in marine methane hydrate environments: impacts on shelf macrobenthic community structure offshore Svalbard. Mar. Ecol. Prog. Ser. 552, 1–18. https://doi.org/10.3354/meps11773.

Åström, E.K., Carroll, M.L., Ambrose Jr., W.G., Sen, A., Silyakova, A., Carroll, J., 2018. Methane cold seeps as biological oases in the high-Arctic deep sea. Limnol. Oceanogr. 63 (S1), S209–S231. https://doi.org/10.1002/lno.10732.

Åström, E.K., Carroll, M.L., Sen, A., Niemann, H., Ambrose Jr., W.G., Lehmann, M.F., Carroll, J., 2019. Chemosynthesis influences food web and community structure in high-Arctic benthos. Mar. Ecol. Prog. Ser. 629, 19–42. https://doi.org/10.3354/meps13101.

Åström, E.K., Sen, A., Carroll, M.L., Carroll, J., 2020. Cold seeps in a warming arctic: insights for benthic ecology. Front. Mar. Sci. 7, 244. https://doi.org/10.3389/fmars.2020.00244.

Baranov, B., Galkin, S., Vedenin, A., Dozorova, A., Gebruk, A., Flint, M., 2020. Methane seeps on the outer shelf of the Laptev Sea: characteristic features, structural control, and benthic fauna. Geo Mar. Lett. 40, 541–557. https://doi.org/10.1007/s00367-020-00655-7.

Boehringer, L., Purser, A., Bergmann, M., Khan, T.M., Schimpf, K., Krämer, C., 2025. Seafloor images and videos collected along OFOBS profile PS143/1_23-1 during RV POLARSTERN cruise PS143/1. PANGAEA. https://doi.org/10.1594/PANGAEA.987478.

Brenke, N., 2005. An epibenthic sledge for operations on marine soft bottom and bedrock. J. Mar. Technol. Soc. 39, 10–19.

Bünz, S., Polyanov, S., Vadakkepuliyambatta, S., Consolaro, C., Mienert, J., 2012. Active gas venting through hydrate-bearing sediments on the vestnesa ridge, offshore W-Svalbard. Mar. Geol. 332–334, 189–197. https://doi.org/10.1016/j.margeo.2012.09.012.

Carroll, M.L., Denisenko, S.G., Renaud, P.E., Ambrose, W.G.J., 2008. Benthic infauna of the seasonally ice-covered western Barents Sea: patterns and relationships to environmental forcing. Deep Sea Res. Part II Top. Stud. Oceanogr. 55, 2340–2351. https://doi.org/10.1016/j.dsr2.2008.05.022.

Chand, S., Knies, J., Geissler, W.H., Plaza-Faverola, A., Thorsnes, T., 2024. Acoustic evidence of hydrocarbon release associated with the spitsbergen transform fault, north of the molloy ridge, Fram Strait. Front. Earth Sci. 12, 1347252. https://doi.org/10.3389/feart.2024.1347252.

Cochrane, S.K.J., Pearson, T.H., Greenacre, M., Costelloe, J., Ellingsen, I.H., Dahle, S., Gulliksen, B., 2012. Benthic fauna and functional traits along a polar front transect in the Barents Sea – advancing tools for ecosystem-scale assessments. J. Mar. Syst. 94, 204–217. https://doi.org/10.1016/j.jmarsys.2011.12.001.

Consolaro, C., Rasmussen, T.L., Panieri, G., 2018. Palaeoceanographic and environmental changes in the eastern fram strait during the last 14,000 years based on benthic and planktonic Foraminifera. Mar. Micropaleontol. 139, 84–101.

Dannheim, J., Contribution of the participants, 2025. The expedition PS148 of the research vessel POLARSTERN to the artic ocean in 2025. In: Bornemann, H. (Ed.), Berichte zur Polar- und Meeresforschung = Reports on polar and marine research, Bremerhaven, Alfred-Wegener-Institut Helmholtz-Zentrum für Polar- und Meeresforschung 803, 137. https://doi.org/10.57738/BzPM_0803_2025.

Dølven, K.O., Ferré, B., Silyakova, A., Jansson, P., Linke, P., Moser, M., 2022. Autonomous methane seep site monitoring offshore western Svalbard: hourly to seasonal variability and associated oceanographic parameters. Ocean Sci. 18 (1), 233–254. https://doi.org/10.5194/os-18-233-2022.

Dreutter, S., Warnke, F., Purser, A., 2020. Multibeam bathymetry raw data (Kongsberg EM 122 entire dataset) of RV MARIA S. MERIAN during cruise MSM95. PANGAEA. https://doi.org/10.1594/PANGAEA.924922.

Dreutter, S., Warnke, F., Dorschel, B., Purser, A., 2022. Multibeam bathymetry processed data (Kongsberg EM 122 entire dataset) of RV MARIA S. MERIAN during cruise

MSM95, fram strait, Arctic Ocean. PANGAEA. https://doi.org/10.1594/PANGAEA.950421.

Durden, J.M., Bett, B.J., Horton, T., Serpell-Stevens, A., Morris, K.J., Billett, D.S.M., Ruhl, H.A., 2016. Improving the estimation of deep-sea megabenthos biomass: dimension to wet weight conversions for abyssal invertebrates. Mar. Ecol. Prog. Ser. 552, 71–79.

Eilertsen, M.H., Kongsrud, J.A., Tandberg, A.H.S., Alvestad, T., Budaeva, N., Martell, L., Ramalho, S.P., Falkenhaug, T., Huys, R., Oug, E., Bakken, T., Høisæter, T., Rauch, C., Carvalho, F.C., Savchenko, A.S., Ulvatn, T., Kongshavn, K., Berntsen, C.M., Olsen, B. R., Pedersen, R.B., 2024. Diversity, habitat endemicity and trophic ecology of the fauna of Loki's castle vent field on the arctic mid-ocean ridge. Sci. Rep. 14 (1), 103. https://doi.org/10.1038/s41598-023-46434-z. PMID: 38167527; PMCID: PMC10761849.

Eilertsen, M.H., Klemetsdal, M.L.B., Kongsrud, J.A., Tandberg, A.H.S., Alvestad, T., Esteban Vasquez, B.L., Savini, A., Argentino, C., Panieri, G., 2025. Faunal communities of arctic deep-water methane seeps are specialised with links to hydrothermal vents. Deep Sea Res. Oceanogr. Res. Pap. 225, 104594. https://doi.org/10.1016/j.dsr.2025.104594.

Folmer, O., Black, M., Hoeh, W., Lutz, R., Vrijenhoek, R., 1994. DNA primers for amplification of mitochondrial cytochrome *c* oxidase subunit I from diverse metazoan invertebrates. Molecular marine biology and biotechnology 3, 294–299.

Gebruk, A.V., Krylova, E.M., Lein, A.Y., Vinogradov, G.M., Anderson, E., Pimenov, N.V., Cherkashev, G.A., Crane, K., 2003. Methane seep community of the Håkon Mosby mud volcano (the Norwegian Sea): composition and trophic aspects. Sarsia 88 (6), 394–403. https://doi.org/10.1080/00364820310003190.

Gorska, B., Gromisz, S., Legeżyńska, J., Soltwedel, T., Włodarska-Kowalczuk, M., 2022. Macrobenthic diversity response to the atlantification of the Arctic Ocean (Fram Strait, 79°N) – a taxonomic and functional trait approach. Ecol. Indic. 144, 109464. https://doi.org/10.1016/j.ecolind.2022.109464.

Hemmateenejad, F., Savini, A., Fallati, L., Bünz, S., Ferré, B., Panieri, G., 2025a. Arctic Ocean and Barents Sea seafloor substrate catalogue: CAGE 15-2. CAGE 17-2; CAGE 18-4; CAGE 18-5; CAGE 20-7; CAGE 21-1 (AKMA); CAGE 22-2 (AKMA/OceanSenses); and AKMA3 cruises, R/V Helmer Hanssen and Kronprins Håkon). https://doi.org/10.7557/7.8034.

Hemmateenejad, F., Ramalho, S.P., Heggernes Eilertsen, M., Straube, N., Vadakkepuliyambatta, S., Waghorn, K., Panieri, G., Bünz, S., Ferré, B., Argentino, C., Alesandra Savini, A., Fallati, L., 2025b. Arctic Ocean and Barents Sea Benthic Faunal and Fish Catalogue, CAGE 15–2. https://doi.org/10.7557/7.8033. CAGE 17-2; CAGE 18-4; CAGE 18-5; CAGE 20-7; CAGE 21-1 (AKMA); CAGE 22-2 (AKMA/OceanSenses); and AKMA3 cruises, R/V Helmer Hanssen and Kronprins Håkon).

Horton, T., Marsh, L., Bett, B.J., Gates, A.R., Jones, D.O.B., Benoist, N.M.A., Pfeifer, S., Simon-Lledó, E., Durden, J.M., Vandepitte, L., Appeltans, W., 2021. Recommendations for the standardisation of open taxonomic nomenclature for image-based identifications. Front. Mar. Sci. 8, 620702. https://doi.org/10.3389/fmars.2021.620702.

Isler, T., Boehringer, L., Purser, A., 2024a. Ocean Floor Observation and Bathymetry System (OFOBS) seafloor images of the Fram Strait collected during RV POLARSTERN cruise PS136 [publication series], PANGAEA. https://doi.org/10.1594/PANGAEA.971365.

Isler, T., Boehringer, L., Purser, A., 2024b. Seafloor Images Collected Along OFOBS Profile PS136_22-1 During RV POLARSTERN Cruise PS136. https://doi.org/10.1594/PANGAEA.971407.

Jakobsson, M., Mayer, L.A., Bringensparr, C., Castro, C.F., Mohammad, R., Johnson, P., Ketter, T., Accettella, D., Amblas, D., An, L., Arndt, J.E., Canals, M., Casamor, J.L., Chauché, N., Coakley, B., Danielson, S., Demarte, M., Dickson, M.-L., Dorschel, B., Dowdeswell, J.A., Dreutter, S., Fremand, A.C., Gallant, D., Hall, J.K., Hehemann, L., Hodnesdal, H., Hong, J., Ivaldi, R., Kane, E., Klaucke, I., Krawczyk, D.W., Kristoffersen, Y., Kuipers, B.R., Millan, R., Masetti, G., Morlighem, M., Noormets, R., Prescott, M.M., Rebesco, M., Rignot, E., Semiletov, I., Tate, A.J., Travaglini, P., Velicogna, I., Weatherall, P., Weinrebe, W., Willis, J.K., Wood, M., Zarayskaya, Y., Zhang, T., Zimmermann, M., Zinglersen, K.B., 2020. The international bathymetric chart of the Arctic Ocean version 4.0. Sci. Data 7, 176. https://doi.org/10.1038/s41597-020-0520-9.

Käß, M., Vedenin, A., Hasemann, C., Brandt, A., Soltwedel, T., 2019. Community structure of macrofauna in the deep Fram Strait: a comparison between two bathymetric gradients in ice-covered and ice-free areas. Deep Sea Res. Oceanogr. Res. Pap. 152, 103102. https://doi.org/10.1016/j.dsr.2019.103102.

Käß, M., Chikina, M., Vedenin, A., Pineda Metz, S., Soltwedel, T., 2021. Traits and drivers: functioning of macrobenthic communities across the deep Fram Strait (Arctic Ocean). Ecol. Indic. 123, 107324. https://doi.org/10.1016/j.ecolind.2020.107324.

Kearse, M., Moir, R., Wilson, A., Stones-Havas, S., Cheung, M., Sturrock, S., Buxton, S., Cooper, A., Markowitz, S., Duran, C., Thierer, T., Ashton, B., Meintjes, P., Drummond, A., 2012. Geneious basic: an integrated and extendable desktop software platform for the organization and analysis of sequence data. Bioinformatics 28, 1647–1649.

Konovalova, O., Rimskaya-Korsakova, N., Kuznetsov, P., Osadchiev, A., Fedyaeva, M., Moiseeva, I., Purgina, D., Kosmach, D., Semiletov, I., 2024. Benthic communities under methane gradient in the Laptev and East Siberian seas. Front. Ecol. Evol. 12, 1406680. https://doi.org/10.3389/fevo.2024.1406680.

Linse, K., Schrade, M., Purser, A., 2026. Ocean floor observation and bathymetry system (OFOBS) in-situ images analyses of benthic fauna abundances and seafloor cover percentage at arctic vestnesa ridge methane seeps collected during the expedition MSM108 in 2022, PS136 in 2023 and PS143/1 in 2024 (version 1.0). UK Polar Data Centr. Nat. Environ. Res. Coun. UK Res. Innov. https://doi.org/10.5285/c56792e3-c94b-4ea5-afb2-72840919b01f.

MacDonald, I.R., Bluhm, B.A., Iken, K., Gagaev, G., Strong, S., 2010. Benthic macrofauna and megafauna assemblages in the arctic deep-sea Canada basin. Deep Sea Res. Part II Top. Stud. Oceanogr. 57 (1–2), 136–152. https://doi.org/10.1016/j.dsr2.2009.08.012.

Mau, S., Römer, M., Torres, M.E., Bussmann, I., Pape, T., Damm, E., Geprägs, P., Wintersteller, P., Hsu, C.-W., Loher, M., Bohrmann, G., 2017. Widespread methane seepage along the continental margin off Svalbard - from Bjørnøya to Kongsfjorden. Sci. Rep. 7 (1). https://doi.org/10.1038/srep42997.

Melaniuk, K., Sztybor, K., Treude, T., Sommer, S., Rasmussen, T.L., 2022. Influence of methane seepage on isotopic signatures in living deep-sea benthic Foraminifera, 79°. NHRI Sci. Rep. 12, 1169. https://doi.org/10.1038/s41598-022-05175-1.

Meyer-Kaiser, K.S., Schrage, K., Bergmann, M., 2025. Hard-bottom communities in the deep Fram strait: patterns, processes, and looming questions. Deep Sea Res. Part II Top. Stud. Oceanogr. 222, 105506. https://doi.org/10.1016/j.dsr2.2025.105506.

Myhre, C.L., Ferré, B., Platt, S.M., Silyakova, A., Hermansen, O., Allen, G., Pisso, I., Schmidbauer, N., Stohl, A., Pitt, J., Jansson, P., Greinert, J., Percival, C., Fjaeraa, A. M., O'Shea, S.J., Gallagher, M., Le Breton, M., Bower, K.N., Bauguitte, S.J.B., Dalsøren, S., Vadakkepuliyambatta, S., Fisher, R.E., Nisbet, E.G., Lowry, D., Myhre, G., Pyle, J.A., Cain, M., Mienert, J., 2016. Extensive release of methane from arctic seabed west of Svalbard during summer 2014 does not influence the atmosphere. Geophys. Res. Lett. 43 (9), 4624–4631. https://doi.org/10.1002/2016gl068999.

Panieri, G., Bünz, S., Fornari, D.J., Escartin, J., Serov, P., Jansson, P., Torres, M.E., Johnson, J.E., Hong, W., Sauer, S., Garcia, R., Gracias, N., 2017. An integrated view of the methane system in the pockmarks at vestnesa ridge, 79°N. Mar. Geol. 390, 282–300.

Panieri, G., Argentino, C., Ramalho, S.P., Vulcano, F., Savini, A., Fallati, L., Brekke, T., Galimberti, G., Riva, F., Balsa, J., Eilertsen, M.H., Stokke, R., Steen, I.H., Sahy, D., Kalenitchenko, D., Büenz, S., Mattingsdal, R., 2024. An arctic natural oil seep investigated from space to the seafloor. Sci. Total Environ. 907, 167788. https://doi.org/10.1016/j.scitotenv.2023.167788.

Panieri, G., Copley, J.T., Linse, K., Nye, V., Ramirez-Llodra, E., Argentino, C., Ferré, B., , the Arctic Deep-Extreme24 consortium, Rogers, A.D., 2025. Seafloor gas hydrate mounds with chemosynthetic fauna at 3640 m deep in the Greenland Sea. Nat. Commun. 16, 11287. https://doi.org/10.1038/s41467-025-67165-x.

Paull, C.K., Dallimore, S.R., Caress, D.W., Gwiazda, R., Melling, H., Riedel, M., Sherman, A., Lundsten, E., Anderson, K., Lundsten, L., Villinger, H., Kopf, A., Johnson, S.B., Hughes Clarke, J., Blasco, S., Conway, K., Neelands, P., Thomas, H., Côté, M., 2015. Active mud volcanoes on the continental slope of the Canadian Beaufort sea. G-cubed 16 (9), 3160–3181. https://doi.org/10.1002/2015GC005928.

Purser, A., Boehringer, L., 2023. FRAM Strait Octopus Observations with Towed Camera: MSM95, MSM108, PS126. Mendeley Data, V1. https://doi.org/10.17632/f96cgnjyty.1.

Purser, A., Marcon, Y., Dreutter, S., Hoge, U., Sablotny, B., Hehemann, L., Lemburg, J., Dorschel, B., Biebow, H., Boetius, A., 2019. Ocean floor observation and bathymetry system (OFOBS): a new towed camera/sonar system for deep-sea habitat surveys. IEEE J. Ocean. Eng. https://doi.org/10.1109/JOE.2018.2794095.

Purser, A., Boehringer, L., Hehemann, L., Hoge, U., Merten, V., Dreutter, S., 2021a. Seabed photographs taken along OFOBS profile MSM95_52-1 during RV MARIA S. MERIAN cruise MSM95. In: Purser, A et al., 2021, OFOBS Seafloor images from the Svalbard Archipelago and Fram Strait, collected during RV MARIA S. MERIAN expedition MSM95 (GPF 19-2_05) [publication series]. PANGAEA. Alfred Wegener Institute, Helmholtz Centre for Polar and Marine Research, Bremerhaven, PANGAEA. https://doi.org/10.1594/PANGAEA.928815.

Purser, A., Hoge, U., Hagemann, J., Lehmenhecker, S., Dauer, E., Korfman, N., Boehringer, L., Merten, V., Priest, T., Dreutter, S., Warnke, F., Hehemann, L., 2021b. Arctic Seafloor Integrity Cruise No. MSM95 – (GPF 19-2_05) doi10.48433%252Fcr_msm95/.

QGIS.org, 2019. QGIS Geographic Information System.

Ramachandran, H., Plaza-Faverola, A., Daigle, H., 2022. Impact of gas saturation and gas column height at the base of the gas hydrate stability zone on fracturing and seepage at vestnesa ridge, west-Svalbard margin. Energies 15, 3156. https://doi.org/10.3390/en15093156.

Rasmussen, T.L., Nielsen, T., 2024. Glacial-interglacial sedimentation control on gas seepage exemplified by vestnesa ridge off NW Svalbard margin. Front. Earth Sci. Sect. Cryosph. Sci. 12. https://doi.org/10.3389/feart.2024.1356341.

Ratnasingham, S., Hebert, P.D.N., 2013. A DNA-based registry for all animal species: the barcode index number (BIN) system. PLoS One 8 (8), e66213. https://doi.org/10.1371/journal.pone.0066213.

Riedel, M., Villinger, H., Freudenthal, T., Pape, T., Bünz, S., Bohrmann, G., 2020. Thermal characterization of pockmarks across vestnesa and svyatogor ridges, offshore Svalbard. J. Geophys. Res. Solid Earth 125. https://doi.org/10.1029/2020JB019468 e2020JB019468.

Rybakova, E., Krylova, E., Mordukhovich, V., 2025. Methane seeps and hydrothermal vents in the Bering Sea: comparative aspects of the fauna, composition and community structure. Reg. Stud. Mar. Sci. 93, 104678. https://doi.org/10.1016/j.rsma.2025.104678.

Sahling, H., Galkin, S.V., Salyuk, A., Greinert, J., Foerstel, H., Piepenburg, D., Suess, E., 2003. Depth-related structure and ecological significance of cold-seep communities—a case study from the Sea of Okhotsk. Deep Sea Res. Oceanogr. Res. Pap. 50 (12), 1391–1409. https://doi.org/10.1016/j.dsr.2003.08.004.

Sahling, H., Römer, M., Pape, T., Bergès, B., dos Santos Fereirra, C., Boelmann, J., Geprägs, P., Tomczyk, M., Nowald, N., Dimmler, W., Schroedter, L., Glockzin, M., Bohrmann, G., 2014. Gas emissions at the continental margin west of Svalbard: mapping, sampling, and quantification. Biogeosciences 11 (21), 6029–6046. https://doi.org/10.5194/bg-11-6029-2014.

Schnier, J., Hasemann, C., Mokievsky, V., Martínez Arbizu, P., Soltwedel, T., 2023. Nematode communities along a bathymetric transect in the deep eastern fram strait (Arctic ocean): interrelations between diversity, function and environment. Front. Mar. Sci. 10. https://doi.org/10.3389/fmars.2023.1271447.

Schulze, A., Halanych, K.M., 2003. Siboglinid evolution shaped by habitat preference and sulfide tolerance. Hydrobiologia 496, 199–205. https://doi.org/10.1023/A:1026192715095.

Sen, A., Himmler, T., Hong, W.L., Chitkara, C., Lee, R.W., Ferré, B., Lepland, A., Knies, J., 2019. Atypical biological features of a new cold seep site on the lofoten-vesterålen continental margin (northern Norway). Sci. Rep. 9 (1), 1762. https://doi.org/10.1038/s41598-018-38070-9.

Shakhova, N., Semiletov, I., Sergienko, V., Lobkovsky, L., Yusupov, V., Salyuk, A., Salomatin, A., Chernykh, D., Kosmach, D., Panteleev, G., Nicolsky, D., Samarkin, V., Joye, S., Charkin, A., Dudarev, O., Meluzov, A., Gustafsson, O., 2015. The East Siberian arctic shelf: towards further assessment of permafrost-related methane fluxes and role of sea ice. Philos. Trans. R. Soc. A Math. Phys. Eng. Sci. 373, 20140451. https://doi.org/10.1098/rsta.2014.0451.

Soltwedel, T., 2023. The expedition PS136 of the research vessel POLARSTERN to the fram strait in 2023. In: Bornemann, H. (Ed.), Berichte Zur Polar- Und Meeresforschung = Reports on Polar and Marine Research, 780. Bremerhaven, Alfred-Wegener-Institut Helmholtz-Zentrum für Polar- und Meeresforschung, pp. 1–121. https://doi.org/10.57738/BzPM_0780_2023.

Soltwedel, T., Bauerfeind, E., Bergmann, M., Budaeva, N., Hoste, E., Jaeckisch, N., Juterzenka, K.v., Matthießen, J., Mokievsky, V., Nöthig, E.-M., Quéric, N., Sablotny, B., Sauter, E., Schewe, I., Urban-Malinga, B., Wegner, J., Wlodarska-Kowalczuk, M., Klages, M., 2005. HAUSGARTEN: multidisciplinary investigations at a deep-sea, long-term observatory in the Arctic Ocean. Oceanography (Wash. D. C.) 18 (3), 46–61. https://doi.org/10.5670/oceanog.2005.24.

Soltwedel, T., Bauerfeind, E., Bergmann, M., Bracher, A., Budaeva, N., Busch, K., Cherkasheva, A., Fahl, K., Grzelak, K., Hasemann, C., Jacob, M., Kraft, A., Lalande, C., Metfies, K., Nöthig, E.-M., Meyer, K., Quéric, N.-V., Schewe, I., Wlodarska-Kowalczuk, M., Klages, M., 2016. Natural variability or anthropogenically-induced variation? Insights from 15 years of multidisciplinary observations at the arctic marine LTER site HAUSGARTEN. Ecol. Indic. 65, 89–102. https://doi.org/10.1016/j.ecolind.201510.001.

Soltwedel, T., Asendorf, A., Barthelmeß, T., Barz, J., Becker, K., Becker, N., Böhringer, L., Brinkmann, T., Dannheim, J., Hagemann, J., Hasemann, C., Hoge, U., Holt, J., Janssen, F., Klüver, T., Kraberg, A., Lehmenhecker, S., Purser, A., Schnier, J., 2018. LTER HAUSGARTEN 2022 Long-Term Ecological Research in the Fram Strait, Cruise No. MSM 108. June 06 – July 03, 2022 Tromsø (Norway) – Tromsø (Norway), p. 47. FRAM 2022.

Soltwedel, T., Boehringer, L., Purser, A., Dreutter, S., Schumacher, M., 2024. Multibeam bathymetry raw data (Kongsberg EM 122 entire dataset) of RV MARIA S. MERIAN during cruise MSM108. PANGAEA. https://doi.org/10.1594/PANGAEA.965808.

Taylor, J., Krumpen, T., Soltwedel, T., Gutt, J., Bergmann, M., 2016. Regional- and local-scale variations in benthic megafaunal composition at the arctic deep-sea observatory HAUSGARTEN. Deep Sea Res. Oceanogr. Res. Pap. 108, 58–72.

Taylor, J., Krumpen, T., Soltwedel, T., Gutt, J., Bergmann, M., 2017. Dynamic benthic megafaunal communities: assessing temporal variations in structure, composition and diversity at the arctic deep-sea observatory HAUSGARTEN between 2004 and 2015. Deep Sea Res. Oceanogr. Res. Pap. 122, 81–94.

Teixidó, N., Garrabou, J., Gutt, J., Arntz, W., 2004. Recovery in antarctic benthos after iceberg disturbance: trends in benthic composition, abundance and growth forms. Mar. Ecol. Prog. Ser. 278, 1–16.

Teixidó, N., Garrabou, J., Gutt, J., Arntz, W., 2007. Iceberg disturbance and successional spatial patterns: the case of the shelf antarctic benthic communities. Ecosystems 10 (1), 143–158.

Thorsnes, T., Chand, S., Bellec, V., Nixon, F.C., Brunstad, H., Lepland, A., Aarrestad, S.M., 2023. Gas seeps in Norwegian waters – distribution and mechanisms. Nor. J. Geol. 103, 202309. https://doi.org/10.17850/njg103-2-4.

Tucker, M., 1991. Sedimentary Petrology: an Introduction to the Origin of Sedimentary Rocks. Blackwell Sciences Ltd, Oxford.

Vedenin, A., Mokievsky, V., Soltwedel, T., Budaeva, N., 2019. The temporal variability of the macrofauna at the deep-sea observatory HAUSGARTEN (Fram strait, Arctic Ocean). Polar Biol. 42, 527–540. https://doi.org/10.1007/s00300-018-02442-8.

Vedenin, A., Kokarev, V.N., Chikina, M.V., Basin, A.B., Galkin, S.V., Gebruk, A.V., 2020. Fauna associated with shallow-water methane seeps in the laptev sea. PeerJ 8, e9018. https://doi.org/10.7717/peerj.9018.

Yusupov, V.I., Salyuk, A.N., Karnaukh, V.N., Semiletov, I.P., Shakhova, N.E., 2010. Detection of methane ebullition in shelf waters of the laptev sea in the Eastern arctic region. In: Doklady Earth Sciences, 430. MAIK Nauka/Interperiodica, pp. 261–264, 2.